UNIVERSITY OF CALIFORNIA, SAN DIEGO

Substructure within the Dorsal Lateral Geniculate Nucleus of the Pigmented Rat

A dissertation submitted in partial satisfaction of the
requirements for the degree
Doctor of Philosophy

in

Neurosciences

by

Claire B. Discenza

Committee in charge:

Professor Pamela Reinagel, Chair
Professor Timothy Genter, Co-Chair
Professor Serge Belongie
Professor Edward Calloway
Professor Maryann Martone

2011

The dissertation of Claire B. Discenza is approved, and it is acceptable in quality and form for publication on microfilm and electronically:

_____

_____

_____

_____
Co-Chair

_____
Chair

University of California, San Diego

2011

DEDICATION

To Skip Lizárd

TABLE OF CONTENTS

LIST OF FIGURES

LIST OF TABLES

LIST OF ABBREVIATIONS

CTb	Cholera Toxin b subunit
DAB	Diaminobenzidine
DAPI	4',6-diamidino-2-phenylindole
dLGN	dorsal Lateral Geniculate Nucleus
DMSO	Dimethyl Sulfoxide
FITC	Fluorescein Isothiocyanate
GABA	Gamma-Aminobutyric Acid
IGL	Intergeniculate Leaflet
IN	intergeniculate Inhibitory Neuron
LGN	Lateral Geniculate Nucleus of the thalamus
RGC	Retinal Gangion Cell
vLGN	ventral Lateral Geniculate Nucleus

ACKNOWLEDGEMENTS

Some or all of the material presented in Chapter 2 may be prepared for submission for publication. Discenza CB & Reinagel P. The dissertation author was the primary investigator and author of this material.

I would firstly like to thank the many people who have supported me throughout my graduate career, both scientifically and personally. In particular, I would like to acknowledge my advisor, Pam Reinagel, and the members of the Reinagel lab for backing me up along every step of this project, and most of all, for believing in me. Same goes for my committee: Tim Gentner, Maryann Martone, Serge Belongie, and Ed Calloway. I would like to thank Harvey Karten and Agnieszka Brzozowska-Prechtl of the Karten lab for teaching me everything I know about histology, as well as more-than-generously allowing me free access to their lab tools, expertise, and workspace. In addition, several other labs deserve more thanks than I can give in this paragraph, for sending aid and resources my way. Among them, I would like to thank Partha Mitra and Vadim Pinskiy of the Mitra lab, Dave Matthews, Jeff Moore, and David Kleinfeld of the Kleinfeld Lab, and Maryann Martone, Hiroyuki Hakozaki, and Stephan Lamont of NCMIR for their instruction, support, and patience throughout data collection and analysis.

I would like to also thank the UCSD Neurosciences program for their support, emotional as well as financial, throughout my graduate career. Special thanks to Anirvan Ghosh, Yishi Jin, Tim Gentner, and Christa Leudeking. And special thanks to Bill Kristan, my 'Spiritual Advisor', for his kindness, advice, and most importantly friendship throughout this whole ordeal.

Second to last, but definitely not second to least, I need to thank my darling friends whom I could never do without (including but not limited to): Amelia Cass, Sam Berliner, Emma Anderson, Christina Woodward, Natalie Stahl, Molly Wright, Hannah Colburn, Nick Wall, Dr. Emily Anderson, Dr. Leif Gibb, Gordy Stephenson, Yaniv Rosen, Marko Lubarda, and Dr. Jeff Gauthier. I love you, guys.

And finally, I would like to thank my family for being so sweet and for setting me off in the first place for some higher quality higher education.

VITA

2002-2003	Technician in the molecular pathology lab of Dr. Simon L. Dove Ph.D., at the Children's Hospital in Boston, MA.
2004	Munno Prize for excellence in Neuroscience Bowdoin College
2005	B.A. in Neuroscience *with Honors* Bowdoin College
2011	Ph.D. in Neurosciences University of California, San Diego

PUBLICATIONS

Davis, J.B., Donahue, R.J., Discenza, C.B., Waite, A.A., & Ramus, S.J., 2006: Hippocampal dependence of anticipatory neuronal firing in the orbitofrontal cortex of rats learning an odor-sequence memory task, *Society for Neuroscience Abstracts*.

Discenza, C.D., Karten H.J. & Reinagel, P., 2008: Anatomical targets of retinal ganglion cell axons in the Long-Evans rat, *Society for Neuroscience Abstracts*.

Ramus, S.J., Davis, J. B., Donahue, R. J., Discenza, C. B. & Waite, A. A. (2007), Interactions between the Orbitofrontal Cortex and the Hippocampal Memory System during the Storage of Long-Term Memory. Annals of the New York Academy of Sciences, 1121: 216-231.

ABSTRACT OF THE DISSERTATION

Substructure within the Dorsal Lateral Geniculate Nucleus of the Pigmented Rat

by

Claire B. Discenza

Doctor of Philosophy in Neurosciences

University of California, San Diego, 2011

Professor Pamela Reinagel, Chair
Professor Timothy Genter, Co-Chair

Much can be learned about the functional organization of the visual system by examining its anatomy. In traditionally-studied cat and primate species, certain morphological types of retinal ganglion cells project to specific thalamic and then cortical layers, separated by eye in each region. In addition, physiology shows that information is segregated by functional cell type; each layer is a complete or near-complete map of some aspect of the world such as form and motion. This results in a system that can easily distribute specialized information without disrupting the larger visuo-spatial map.

While the layers of the macaque retino-recipient thalamus are easily discernible due to the correlation between cytoarchitecture and function, the rat

geniculate appears to have no such patterning. As the rat is a favorable research model, it is important to understand how its brain is set up to tackle the same visual problems as that of higher mammals.

The purpose of this project was to describe substructure within the rat dorsal lateral geniculate nucleus of the thalamus, with the goal of learning more about how the anatomical organization might give insight into function. To visualize the anatomy, I intra-occularly injected retrograde tracer to map retinal termini throughout the nucleus. Based on three-dimensional reconstructions of termination zones from each eye, I identified multiple ipsilaterally-recipient zones within the largely contralateral thalamic nucleus. These ipsilateral subregions are more reminiscent of the layering in the primate thalamus than previously described in the rat. Furthermore, the nucleus appears to be well segregated by eye, suggesting that, like in these other species, the rat thalamus passes on information without binocular mixing.

My findings also support the hypothesis that, unlike in the primate, rat cell bodies throughout the layers appear to be cytoarchitecturally homogeneous. While we can glean insight into the function of macaque thalamic layers by looking at cell-body statistics such as size and density, no such patterns can be seen in the rat. Among other possibilities, this could mean that rat projection neurons have similar morphologies, or that functional cell types are intermingled and not spatially organized as they are in other species.

Chapter 1

Introduction

1.1 Basic organization of the mammalian dorsal lateral geniculate nucleus of the thalamus

How photons give rise to a consistent and integrated visual world has been a major question in neuroscience since the field began. Now we know that the brain uses diverse sets of circuits to get there. From the phototransducing rods and cones and their supporting neurons, many specialized types of projecting retinal ganglion cells take visual signals and spread them to different primary and secondary targets throughout the brain. Some process sight for balance, movement coordination, entraining daily bodily rhythms, and for visual reflexes. Others organize information for object and form recognition.

When we talk about the latter types of vision, we are referring to the streams of information that, after leaving the retina, first pass through each of the bilateral dorsal lateral geniculate nuclei of the thalamus (dLGN) before connecting to the visual cortex and beyond (Sherman and Guillery, 1996; Heggelund, 2003; Jones, 2007, for review). Being a bilateral structure, each of the two dLGN are responsible for processing and relaying half the visual information received by the animal. The way the system is set up, all of the information from the left half of the visual world (mostly from the left eye) crosses at the optic chiasm and goes to the right dLGN, while the right visual hemifield (mostly from the right eye) goes to the left dLGN. However, there is some overlap between what the right and

the left eyes see; even mammals with eyes offset on the sides of their heads have a small portion of the visual field in front of their noses that can be seen by both eyes. This means that each dLGN gets a smaller projection from the same-side eye to complete the picture of that hemifield.

Because the dLGN is the first step in the striato-cortical visual pathway to deal with this binocular input from both retinas (See Rodieck, 1979, for review), it is therefore the first location to handle one of the major problems in vision: how to pass sensory information through the brain while still maintaining local spatial relationships. Besides dealing with input from both eyes, the dLGN also has to handle information from many different functional types of retinal ganglion cells within each eye (Enroth-Cugell and Robson, 1966; Clelend and Levick, 1974; for review see Shapely and Perry, 1986; Rodieck, 1979). How the nucleus organizes, processes, and transmits binocular retinotopic information from diverse ganglion cells teaches us not only about the visual system, but also about the patterns governing the propagation of topographically-organized sensory information in general.

We know quite a bit about how some mammals solve this problem. Most studies of the dLGN have been done in primate and carnivore species, specifically the macaque monkey, *Macaca mulatta*, and the domestic cat, *Felis catus*. Each specie has a different thalamic nuclear structure but the same general organizing principles (for review see Jones, 2007). One major principle is that of the separation and isolation of different types of visual information.

These different types of information originate from the multiple functional types of ganglion cells in the retina. Each ganglion cell type processes visual signals in their receptive fields, or areas of the world from which they sample, in very specific ways. Some ganglion cells detect changes in luminance, some are good edge detectors, some are specialized for motion, and others, for color (see Rodieck, 1979; Shapely and Perry, 1986). Each different ganglion cell type sampling from one location in visual space projects to one corresponding region of the dLGN within a few hundred microns of the termini from other cells sampling from that same visual location. (Sanderson, 1971; Sur and Sherman, 1982; Roe et al.,1989). Within this dLGN region there is very little convergence of retinal

input onto thalamic cells. One dLGN cell receives input from only around one to five retinal cells (Levick et al., 1972) terminating close to their cell bodies (Hamos et al., 1985; Montero, 1991), and retains many properties from these retinal cells even during thalmic processing (Cleland et al., 1971a; Troy, 1983). Each separate visual channel is therefore relayed almost completely independently from the others (Horton and Sherk 1984, Roy et al., 2009).

In addition to the separation of these specialized channels, each dLGN maintains strict separation of information from each eye. In the mature brain of most well-studied mammalian species, the nucleus achieves this by layering input from one eye over the other in zones separated by eye-of-origin (see Jones, 2007; So, 1990). Each layer maintains the spatial mapping conferred from the retina which innervates it, and shares many of the properties of the retinal ganglion cell type from which it samples (Cleland et al., 1971a; Troy, 1983).

Besides receiving and maintaining this pathway segregation within the nucleus, the dLGN also relays its information to specific regions and subregions of the cortex – again maintaining the isolated nature of these pathways. Different functional pathways terminate in separate columns of the visual cortex (Mountcastle, 1957; Lund et al., 1979; Hirsch and Martinez, 2006; for review see Sherman and Guillery, 1996). Each column is sometimes further separated by eye-of-origin into ocular dominance columns, where input from each eye is interleaved (for review, see Jones, 2007). And again, retinotopy is preserved, with neighboring locations of visual space mapping onto neighboring regions of cortical space (Garey and Powell, 1967; Bullier et al., 1984).

Although the functional significance of this cortical architecture is still a mystery (Hubel and Wiesel,1974; for review see Da Costa and Martin, 2010; Horton and Adams, 2005), one theory holds that, due to this organization, cortical neurons can easily sample from, process, and pass on one specific type of information from one particular region of visual space, regardless of eye (Hubel and Wiesel, 1963). Because the cortex is responsible for sending signals to many areas of the brain serving many distinct purposes for the animal, it would be advantageous for the cortex to preserve this structure in the visual signals it receives for the sake of economy.

In this way, most mammals solve the problem of how to handle binocular information by creating a laminar/columnar dLGN that projects to a laminar/columnar cortex. Much of what we know about the function of the cells in these layers and columns comes from physiologically recording from the cells in question. However, anatomy has given us many clues about why and how the system might be set up as it is.

1.2 Anatomical clues to functional organization

In most traditionally-studied visual mammals, this layering in the dLGN can be seen from anatomy alone. In the 1880s and 90s, more than fifty years before Hubel and Wiesel conducted their famous physiological classification of retinal ganglion and thalamic cells (Hubel and Wiesel, 1960; Wiesel, 1960), the anatomist Ramón y Cajal had already described cells by their morphology and posed the basic questions about how these cells might give rise to the perception of a consistent visual world (Ramón y Cajal, 1898; for review see Llinás, 2003). Cajal's anatomical description of the pathways from the eye to the visual cortex inspired many experimentalists, and in effect, started the discussion about the workings of vision.

Since Cajal, the brains of sight-dependent mammals such as primates and carnivores have provided good examples of anatomy supporting function. In primates, some carnivores and some rodents, the lamination of the dLGN can be seen by eye alone, using a nissl-body or horseradish peroxidase stain (Clark, 1932; Clark and Gros,1941; Kaas et al., 1972, 1978). The macaque, for example, has 6 overtly visible layers, each of which receive information from one type of retinal ganglion cell from one eye. Two of these layers, the magnocellular layers, receive information from M ganglion cells (Perry et al.,1984). Like their corresponding retinal cells, magnocellular thalamic cells have on/off spatially opponent receptive fields, and can be easily distinguished from other dLGN cells due to their large soma size and deep nissl staining (see Jones, 2007 for review). The other four layers, the parvocellular layers, sample from P retinal ganglion cells (Shapley and Perry, 1986). The cells, which are much smaller and more weakly stained in nissl

dLGN preparations, have chromatic opponency and small receptive field centers, therefore rendering them sensitive to color and detail. In the primate, these layers are farther divided into ganglion cell receptive field subtype. For example, some ganglion cells increase their firing rate to spots of light illuminating their centers (on-center), and others increase their firing rate to darkness in their center (off-center). The parvo- layers in many primates can be divided farther into sublayers specialized for these off-center or on-center cells, which in some cases can also be disambiguated by anatomy alone (Schiller and Malpeli, 1978; Szmajda et al., 2006).

The carnivore dLGN is also a functionally organized, overtly layered structure in much the same style as that of the primate (Kaas et al., 1972; Guillery 1970). It is, in general, made up of 4-6 contra- or ipsi-only layers, the first two of which (layers A and A1) contain large-to-medium sized cells that are innervated by X and Y retinal ganglion cells. The next layer, layer C, contains large, deeply-staining cells that get their information from Y ganglion cells. The remaining layers, C1 and C2, have small, weakly-staining cells that are W-cell innervated. X cells have slower conductances and sustained responses, whereas Y cells are faster but transient (Enroth-Cugell and Robson, 1966; Cleland et al., 1971). W cells have large receptive fields and slow responses, as well as slow conducting axons (Stone and Fukuda, 1974; Cleland and Levick, 1974b). Additionally, as seen in the primate, these layers are retinotopically organized (for example, Eysel and Wolfhard, 1983; Sanderson, 1971).

While much has been learned about the general organizing principles of the mammalian dLGN from the primate and the carnivore, less is known about the rodent dLGN, or about the differences between the rodent and these higher mammalian species.

1.3 The rat dLGN

The laboratory rat, *Rattus norvegicus*, has been a choice model for many areas of neuroscience research for years, due to the rodent's captive breeding fitness, its small size, and its ability to learn and carry out a variety of tasks in a

controlled laboratory setting. Scientists also favor the rat due to the immense collective knowledge of the anatomy, chemistry, and physiology of its nervous system. The rat's excellent research infrastructure includes commercially available defined strains, established husbandry and veterinary standards, sequenced genomes, and sterotaxic atlases. Although genetic research in rats has been more limited than in mice, some mutant and transgenic lines are available, and in utero electroporation and viral vectors can be used to express exogenous transgenes in specific cells (Lo-Turco, 2009; Short et al., 2004). For these reasons among others, many research laboratories prefer studying rats to other mammals.

However, the rat has historically been a less favored model when it comes to studying vision. Until relatively recently, rats have been regarded as largely non-visual animals, and perhaps due to their nocturnality, are able to use sense of smell and whisker-touch exclusively to navigate their environments (Hutson and Masterson, 1986; Hill and Best, 1981; Carvell and Simons, 1990; Maaswinkel and Whishaw, 1999; Wallace et al., 2002; Markus et al., 1994; Kulvicius et al., 2008; Save et al., 2000). Yet despite their poor acuity and limited color vision (Jacobs, 2001; Prusky et al., 2002, for review, see Burn, 2008), pigmented rats are still able to learn and retain a variety of visual tasks. In the laboratory setting, rats have demonstrated visuo-spatial learning and memory (Zoladek and Roberts, 1978; Morris, 1984), navigation (Mallot et al, 2004), and visual object detection and pattern discrimination (Meir and Reinagel, 2011; Zoccolan et al., 2009; Thompson and Solomon, 1954), as well as visually-mediated fear conditioning (Shi and Davis, 2001) and eye-reflexes and movements such as nystagmus and saccades (Hess et al.,1985; Hikosaka and Sakamoto, 1987; Fuller, 1985).

It is therefore somewhat puzzling that the rat, a mammal that can and does use sight to explore and navigate its environment, should have a fundamentally different visual system from the cat and primate. But indeed, the rat dLGN appears to have several major anatomical and perhaps functional organizational differences.

Firstly, the rat seems to lack the spatial separation of visual pathways that are easily visible in the primate and carnivore. Both the mouse and rat dLGN look homogeneous in a nissl preparation. They appear to lack the cytoarchitec-

trual subdivisions that we see between the magno- and parvocellular layers of the macaque (Reese and Cowey, 1983). In addition, when retinal ganglion cells are traced, input from the ipsilateral eye seems to terminate onto one non-descript ipsilateral region within the largely contralaterally-recipient structure (see Jones, 2007 for review).

It has also been suggested that rat dLGN might not isolate input from the two eyes in the same manner or to the same degree as primate and carnivore. For example, one study found approximately 63% of relay cells respond to stimulation in both eyes, something not seen in other species (Greive, 2005). Furthermore, a significant proportion of cells in the temporal retina project bilaterally, and these cells terminate in the general temporal region of the dLGN that collects information from both eyes (Lund et al., 1974, Jeffrery et al., 1981; Kondo et al., 1993; Reese, 1988). In addition, rat cortical cells also tend not show the strict segregation of different types of information as seen in cat or monkey, and do not show binocular segregation (Ohki et al., 2005; Maffei et al., 1992). Taken together, these results suggest, although not conclusively, that the rat may handle the organization of parallel binocular streams in a very different way than more traditionally-studied mammals.

Yet there have been studies suggesting that rodent dLGN do have spatially-separated lamina functionally organizing retinal inputs, just not layers that are easily visible. In the rat, the idea of 'hidden lamination' has been discussed in the literature for years (see Reese, 1988 for review), for although early studies of the anatomy of the rat dLGN found no cytoarchitecturally-distinct laminae, several distinctive features within the nucleus have been identified both anatomically and physiologically. Running just below the lateral optic tract around the dLGN lies a region receiving input from the optic tectum (Harting et al., 1991). This region is innervated by different morphological retinal ganglion cell types than the rest of the nucleus (Fakuda, 1976; Martin, 1986; see Reese, 1988). In addition, feedback from the cortex is organized topographically as they are in other species (Updyke, 1975; Sefton et al., 1981), Whether these correspond to functional layers remains to be seen. In the mouse, a species much better suited to genetic methods, recent studies have found functional ganglion cell subtypes projecting to layers in the

dLGN (Grubb, 2004; Huberman et al., 2008; Huberman et al., 2009). This leads us to believe that the same would be true in the rat.

1.4 Conclusion

The motivation for the following study is two-fold. Firstly, as the rat has been and continues to be a valuable model for vision, it is imperative that we understand not only how the neurons in the visual nuclei respond to stimuli and process information, but also how they connect with one-another. Only in the context of connectivity can the encoding of the visual world make sense. And secondly, from a comparative anatomy standpoint, it is interesting to see how different species coming from different visual backgrounds and with different demands solve similar problems. For example, it could be the case that rodents and carnivores combine information from the two eyes in a fundamentally different way, putting different demands on the cortex and the geniculate.

In the following chapter, I attempt to address the questions posed here: the question of eye-of-origin input segregation and that of putative ipsilaterally-recipient subregions within the rat dLGN. I will ask whether any cytoarchitectural differences and topographic separation between these subregions might give hints as to whether the rat follows the same geniculate organizational principles as do other visual mammals.

1.5 References

Bullier, J., Kennedy, H., & Salinger, W. (1984) Bifurcation of subcortical afferents to visual areas 17, 18 and 19 in the cat cortex. J. Comp. Neurol. 228: 309-328.

Burn, C. (2008). What is it like to be a rat? Rat sensory perception and its implications for experimental design and rat welfare. Applied Animal Behaviour Science. 112: 1-32.

Carvell, G. E., & Simons, D. J. (1990). Biometric analyses of vibrissal tactile discrimination in the rat. The Journal of Neuroscience. 10(8): 2638-2648.

Clark, W.E. (1932). A morphological study of the lateral geniculate body. Brit. J. Ophthal. 16(5):264-284.

Clark, W. E., & Gros, L.E. (1941). The laminar organization and cell content of the lateral geniculate body in the monkey. J.Anat., Lond. 75: 419-433.

Cleland, B.G., DuIbin, M.W. & Levick, W. R. (1971). Simultaneous recording of input and output of lateral geniculate neurones. Nature, Lond. 231: 191-192.

Cleland B.G., Dubin, M.W., & Levick, WR (1971) Sustained and transient neuroues in the cat's retina and lateral geniculate nucleus. J Physiol (Lond) 217: 473-496

Cleland B.G., & Levick W.R., (1974a). Brisk and sluggish concentrically organized ganglion cells in the cat's retina. J Physiol. 240: 421-456.

Cleland, B.G., & Levick, W.R. (1974b) Properties of rarely encountered types of ganglion cells in the cat's retina and an overall classification. J. Physiol. (Lond.) 240: 457-492.

Da Costa N. M., & Martin K. A. C. (2010). Whose cortical column would that be? Front. Neuroanat. 4:16.

Eysel, U., & Wolfhard, T.H. (1983). Morphological fine tuning of retinotopy within the cat lateral geniculate nucleus. Neurosci. Lett. 39:15-20.

Enroth-Cugell, C., & Robson., J.G. (1966). The contrast sensitivity of retinal ganglion cells of the cat. J. Physiol. 187: 517-552.

Fukuda, Y. (1977). A three-group classification of rat retinal ganglion cells: Histological and physiological studies. Brain Research, 119(2), 327-344.

Fuller, J. H. (1985). Eye and head movements in the pigmented rat. Vision Research, 25(8): 1121-1128.

Garey, L.J., & Powell, T.P.S. (1967). The projection of the lateral geniculate nucleus upon the cortex in the cat. Proc. roy. Soc. B. 169: 107-126.

Grieve, K. L. (2005). Binocular visual responses in cells of the rat dLGN. The Journal of Physiology. 566: 119-124.

Grubb, M.S., & Thompson, I.D. (2004). Biochemical and anatomical subdivision of the dorsal lateral geniculate nucleus in normal mice and in mice lacking the beta2 subunit of the nicotinic acetylcholine receptor. Vision Res. 44: 3365-3376.

Guillery, R.W. (1970). The laminar distribution of retinal fibers in the dorsal lateral geniculate nucleus of the cat. J. comp. Neurol. 138: 339-368.

Hamos, J.E., Van Horn, S.C., Raczkowski, D., Uhlrich, D.J. & Sherman, S.M. (1985). Synaptic connectivity of a local circuit neurone in lateral geniculate nucleus of the cat. Nature. 317:618-621.

Harting, J.K., Huerta, M.F., Hashikawa, T., Van Leishout, DP. (1991). Projection of the mammalian superior colliculus upon the dorsal lat- eral geniculate nucleus: organization of tectogeniculate pathways in nineteen species. J. Comp. Neurol. 304:275Ð306.

Heggelund, P. (2003). Signal processing in the dorsal Lateral Geniculate Nucleus. In G.T. Buracas et. al. (Eds.), Modulation of Neuronal Responses: Implications for Active Vision (109-164). Amsterdam: IOS Press.

Hess, B. J., Precht, W., Reber, A., & Cazin, L. (1985). Horizontal optokinetic ocular nystagmus in the pigmented rat. Neuroscience. 15(1): 97-107.

Hikosaka, O., & Sakamoto, M. (1987). Dynamic characteristics of saccadic eye movements in the albino rat. Neuroscience Research. 4(4): 304-308.

Hill, A. J., & Best, P. J. (1981). Effects of deafness and blindness on the spatial correlates of hippocampal unit activity in the rat. Experimental Neurology. 74(1): 204-217.

Hirsch, J.A., & Martinez, L.M. (2006). Laminar processing in the visual cortical column. Curr Opin Neurobiol. 16: 377-384.

Horton, J.C. & Adams, D.L. (2005). The cortical column: a structure without a function. Philos. Trans. R. Soc. Lond. B Biol. Sci. 360: 837-862.

Horton, J., & Sherk, H. (1984). Receptive field properties in the catÕs lateral geniculate nucleus in the absence of on-center retinal input. J Neurosci. 4:374-380.

Huberman, A. D., Manu, M., Koch, S. M., Susman, M. W., Lutz, A. B., & Ullian, E. M. (2008). Architecture and activity-mediated refinement of axonal projections from a mosaic of genetically identified retinal ganglion cells. Neuron. 59(3): 425-438.

Huberman, A. D., Wei, W., Elstrott, J., Stafford, B. K., Feller, M. B., & Barres, B. A. (2009). Genetic identification of an on-off direction- selective retinal ganglion cell subtype reveals a layer-specific subcortical map of posterior motion. Neuron. 62(3): 327-334.

Hubel, D.H. (1960). Single unit activity in lateral geniculate body and optic tract of unrestrained cats. J Physiol. 150: 91-104.

Hubel, D. H., & Wiesel, T. N. (1963). Shape and arrangement of columns in cat's striate cortex. J. Physiol. 165: 559-568.

Hubel, D.H. & Wiesel, T.N. (1974). Uniformity of monkey striate cortex: a parallel relationship between field size, scatter, and magnification factor. J Comp Neur. 158: 295-306.

Hutson, K. A., & Masterton, R. B. (1986). The sensory contribution of a single vibrissa's cortical barrel. Journal of Neurophysiology. 56(4): 1196-1223.

Jacobs, G. H., Fenwick, J. A., & Williams, G. A. (2001). Cone-based vision of rats for ultraviolet and visible lights. The Journal of Experimental Biology. 204: 2439-2446.

Jeffery, G., Cowey, A., & Kuypers, H. G. (1981). Bifurcating retinal ganglion cell axons in the rat, demonstrated by retrograde double labelling. Experimental Brain Research. 44(1): 34-40.

Jones, E. G. (2007). The Thalamus. New York, NY: Cambridge University Press.

Kaas, J.H., Guillery, R.W. & Allman, J.M. (1972). Some principles of organization in the dorsal lateral geniculate nucleus. Brain, Behav. Evol. 6: 253-299.

Kaas, J.H., Huerta, M.F., Weber, J.T., & Harting, J.K. (1978). Patterns of retinal terminations and laminar organization of the lateral geniculate nucleus of primates. J. Comp. Neurol. 182: 517-553.

Kondo, Y., Takada, M., Honda, Y., & Mizuno, N. (1993). Bilateral projections of single retinal ganglion cells to the lateral geniculate nuclei and superior colliculi in the albino rat. Brain Research. 608(2): 204-215.

Kulvicius, T., Tamosiunaite, M., Ainge, J., Dudchenko, P., & Worgotter, F. (2008). Odor supported place cell model and goal navigation in rodents. Journal of Computational Neuroscience. 25(3): 481-500.

Levick, W. R., Cleland, B. G. & Dublin, M. W. (1972) Lateral geniculate neurons of cat: retinal inputs and physiology. Invest. Ophthalmol. 11(5): 302-311.

Llinás, R.R. (2003). The contribution of Santiago Ramón y Cajal to functional neuroscience. Nat Rev Neurosci. 4: 77-80.

LoTurco, J., Manent, J.B., & Sidiqi, F. (2009). New and improved tools for in utero electroporation studies of developing cerebral cortex. Cereb Cortex. 19: 120-125.

Lund, J. S., Henry, G. H., Macqueen, C. L., & Harvey, A. R. (1979). Anatomical orginization of the primary visual cortex (area 17) of the cat: A comparison with area 17 of the macaque monkey. J. Compo Neurol. 184: 599-618.

Lund, R.D., Lund, J.S., & Wise, R.P. (1974). The organization of the retinal projection to the dorsal lateral geniculate nucleus in pigmented and albino rats. J. comp. Neurol. 158: 384-404.

Maaswinkel, H., & Whishaw, I. Q. (1999). Homing with locale, taxon, and dead reckoning strategies by foraging rats: Sensory hierarchy in spatial navigation. Behavioural Brain Research. 99(2): 143-152.

Maffei, L. ,Berardi, N. , Domenici, L. , Parisi, V. &Pizzorusso, T. (1992). Nerve Growth Factor (NGF) prevents the shift in ocular dominance distribution of visual cortical neurons in monocularly deprived rats. Journal of Neuroscience. 12: 4651-4662.

Markus, E. J., Barnes, C. A., McNaughton, B. L., Gladden, V. L., & Skaggs, W. E. (1994). Spatial information content and reliability of hippocampal CA1 neurons: Effects of visual input. Hippocampus. 4(4): 410-421.

Fukuda, Y. (1977). A three-group classification of rat retinal ganglion cells: Histological and physiological studies. Brain Research, 119(2), 327-344.

Meier, P., & Reinagel, P. (2011). Rat performance on visual detection task modeled with divisive normalization and adaptive decision thresholds. Journal of Vision. 11(9):1Ð17.

Montero, V. M. (1991). A quantitative study of synaptic contacts on interneurons and relay cells of the cat lateral geniculate nucleus. Exp. Brain Res. 86: 257-270.

Morris, R. (1984). Developments of a water-maze procedure for studying spatial learning in the rat. Journal of Neuroscience Methods. 11(1): 47-60.

Mountcastle, V.B. (1957). Modality and topographic properties of single neurons of cat's somatic sensory cortex. J. Neurophys. 20: 408-434.

Ohki, K., Chung, S., Ch'ng, Y.H., Kara, P., & Reid, C. (2005) Functional imaging with cellular resolution reveals precise microarchitecture in visual cortex. Nature 433: 597Ð603.

Perry, V.H., Oehler, R., & Cowey, A. (1984). Retinal ganglion cells that project to the dorsal lateral geniculate nucleus in the macaque monkey. Neuroscience. 12(4): 1101-1123.

Prusky, G. T., Harker, K. T., Douglas, R. M., & Whishaw, I. Q. (2002). Variation in visual acuity within pigmented, and between pigmented and albino rat strains. Behavioural Brain Research, 136(2), 339-348.

Ramón y Cajal, S. (1898). Estructura del quiasma optico y teoria general de los entrecruzamientos de las vias nerviosas. Rev. Trim. Micrografica. núm. 1.

Reese, B. E., & Cowey, A. (1983). Projection lines and the ipsilateral retinogeniculate pathway in the hooded rat. Neuroscience. 10(4): 1233-1247.

Reese, B. E. (1988). 'Hidden laminationÕ in the dorsal lateral geniculate nucleus: The functional organization of this thalamic region in the rat. Brain Research Reviews. 13(2): 119-137.

Rodieck, R.W. (1979). Visual pathways. Annual Review of Neuroscience. 2(1): 193-225.

Roe, A. W., Garraghty, P. E. & Sur, M. (1989). Terminal arbors of single ON-center and OFF-center X and Y retinal ganglion cell axons within the ferret's lateral geniculate nucleus. J. Comp. Neurol. 288: 208-242.

Roy, S., Jayakumar, J., Martin, P.R., Dreher, B., Saalmann, Y.B., Hu, D., & Vidyasagar, T.R. (2009). Segregation of short-wavelength-sensitive (S) cone signals in the macaque dorsal lateral geniculate nucleus. Eur J Neruosci. 30(8): 1517-1526.

Sanderson, K.J. (1971). Visual field projection columns and magnification factors in the lateral geniculate nucleus of the cat. Exp Brain Res. 13: 159-177.

Save, E., Nerad, L., & Poucet, B. (2000). Contribution of multiple sensory information to place field stability in hippocampal place cells. Hippocampus. 10(1): 64-76.

Schiller, P.H., & Malpeli, J.G. (1978). Functional specificity of lateral geniculate nucleus laminae of the rhesus monkey. J Neurophysiol. 41: 788-797.

Sefton, A.J., Mackay-Sim, A., Baur, A., & Cottee, L.J. (1981). Cortical projections to visual centres in the rat: An HRP study. Brain Res. 215: 1-13.

Shapley, R.M., & Perry, V.H. (1986). Cat and monkey retinal ganglion cells and their visual functional roles. Trends Neurosci. 9: 1-7.

Sherman, S.M., &Guillery, R.W. (1996). Functional organization of thalamocortical relays. Journal of Neurophysiology. 76: 1367-1395.

Shi, C., & Davis, M. (2001). Visual pathways involved in fear conditioning measured with fear-potentiated startle: Behavioral and anatomic studies. The Journal of Neuroscience. 21(24): 9844-9855.

Short, M.P., Choi, B.C., Lee, J.K., Malick, A., Breakefield, X.O., & Martuza, R.L. (2004). Gene delivery to glioma cells in rat brain by grafting of a retrovirus packaging cell line. Journal of Neuroscience Research. 27(3): 427-439.

So, K.F., Campbell, G., & Lieberman, A.R. (1990). Development of the mammalian retinogeniculate pathway: target finding, transient synapses, and binocular segregation. J Exp Biol. 153: 85-104.

Stone, J., & Fukuda, Y. (1974). Properties of cat retinal ganglion cells: A comparison of W-cells with X- and Y-cells. J. Neurophysiol. 37: 722-748.

Sur, M., & Sherman, S.M. (1982). Retinogeniculate terminations in cats: Morphological differences between X and Y cell axons. Science. 218: 389- 391.

Szmajda, B.A., Buzas, P., FitzGibbon, T., & Martin, P.R. (2006). Geniculocortical relay of blue-off signals in the primate visual system. Proc Natl Acad Sci. 103: 19512-19517.

Thompson, W. R., & Solomon L. M. (1954). Spontaneous pattern discrimination in the rat. Journal of Comparative and Physiological Psychology. 47(2): 104-107.

Troy, J.B. (1983). Spatial contrast sensitivities of X and Y type neurones in the cat's dorsal lateral geniculate nucleus. J Physiol. 344: 397-417.

Updyke, B.V. (1975). The patterns of projection of cortical areas 17, 18 and 19 onto the laminae of the dorsal lateral geniculate nucleus in the cat. J Comp Neurol. 163: 377-395.

Wallace, D. G., Hines, D. J., Pellis, S. M., & Whishaw, I. Q. (2002). Vestibular information is required for dead reckoning in the rat. The Journal of Neuroscience. 22(22): 10009-10017.

Wiesel, T.N. (1958). Recording inhibition and excitation in the cat's retinal ganglion cells with intracellular electrodes. Nature, Lond. 183: 264-265.

Wiesel, T.N. (1960). Receptive fields of ganglion cells in the cat's retina. J. Physiol. 153: 583-594.

Zoccolan, D., Oertelt, N., DiCarlo, J. J., & Cox, D. D. (2009). A rodent model for the study of invariant visual object recognition. Proceedings of the National Academy of Sciences of the United States of America, 106(21): 8748-8753.

Zoladek, L. &W.A. Roberts. (1978). The sensory basis of spatial memory in the rat. Anim. Learn. Behav. 6: 77-81.

Chapter 2

Dorsal Lateral Geniculate Substructure in the Long-Evans Rat: a Cholera Toxin B Subunit Study

2.1 Abstract

The purpose of this study was to describe the substructure of the rat dorsal lateral geniculate nucleus of the thalamus based on the eye-of-origin of its retinal ganglion cell inputs. While more traditionally studied visual mammals such as cat and primate show distinct lamination of parallel pathways – each geniculate layer a retinotopic map of some aspect of the visual world – such lamination is not overt in the rat. To examine the cytoarchitecture here, we made intra-ocular injections of the fluorophor-conjugated B-subunit of cholera toxin, a sensitive anterograde tracer. We injected this dye bilaterally or unilaterally in the vitreous of adult male Long-Evans rats, and nissl-stained for cell somas. After sectioning, we imaged using high-throughput sub-micron resolution scanners. By outlining all regions of retinal termini, we located on average three relatively conserved ipsilateral-recipient zones within each dominantly contralateral-recipient nucleus. Aligning these images and making three-dimensional reconstructions of these regions gave

us a more detailed picture of the retinal projection fields throughout the nucleus. In addition, using these projection-defined outlines and nissl images, we were able to calculate cell-soma statistics such as orientation and density. Our results support the hypothesis that, unlike the geniculate laminae observed in other species, the putative subregions within the rat dorsal lateral geniculate show no cytoarchitectural differences among the properties studied. However, by comparing the eye inputs between subjects and looking at the segregation of dye throughout the nucleus, our data nevertheless support the idea of well-segregated 'hidden laminae' in the rat dorsal lateral geniculate.

2.2 Introduction

The laboratory rat (*Rattus norvegicus*) has been a choice model for many areas of neuroscience research for years, due to the rodent's captive breeding fitness, its small size, and its ability to learn and carry out a variety of tasks in a controlled laboratory setting. Scientists also favor the rat due to the immense collective knowledge of the anatomy, chemistry, and physiology of its nervous system. For these reasons among others, many research laboratories prefer studying rats to other mammals.

However, the rat has been a less favored model when it comes to studying vision. Until relatively recently, rats have been regarded as largely non-visual animals, and perhaps due to their nocturnality, are able to use sense of smell and whisker-touch exclusively to navigate their environments (Hutson and Masterson, 1986; Hill and Best, 1981; Carvell and Simons, 1990; Maaswinkel and Whishaw, 1999; Wallace et al., 2002; Markus et al., 1994; Kulvicius et al., 2008; Save et al., 2000). Yet despite their poor acuity and limited color vision (Jacobs et al., 2001; Prusky et al., 2002, for review see Burn, 2008), pigmented rats are still able to learn and retain a variety of visual tasks. In the laboratory setting, rats have demonstrated visuo-spatial learning and memory (Zoladek and Roberts, 1978; Morris, 1984), navigation (Mallot et al, 2004, Holscher et al., 2005), and visual object detection and pattern discrimination (Meier and Reinagel, 2011; Zoccolan et al., 2009; Thompson and Solomon, 1954), as well as visually-mediated fear condition-

ing (Shi and Davis, 2001) and eye-reflexes and movements such as nystagmus and saccades (Hess et al.,1985; Hikosaka and Sakamoto, 1987; Fuller, 1985).

In addition to exhibiting visually-guided behaviors, rat visual physiology has been shown to be similar in many respects to the more traditionally studied cats and primates, from which most of our knowledge has been gleaned. In particular, the dorsal lateral geniculate nucleus (dLGN) of the visual thalamus is comprised of the same basic categories of cells. The dLGN contains GABA-ergic intrageniculate inhibitory interneurons that receive and modify visual signals by projecting back onto the nucleus, as well as glutamatergic excitatory relay cells that pass information from the eye onto secondary visual targets such as the cortex and the thalamic reticular nucleus (see Tsumoto, 1990 for review). These excitatory cells have several functional modes, a single-spiking and a bursting state, allowing them to relay different types of information to their targets (Guido et al.,1992; Lu et al.,1992). Thus the basic workings of this thalamic nucleus appears to be the same in rodents, primates, and carnivores (see Jones, 2007, for review).

This current study aims to help farther our anatomical knowledge of the rat visual system by exploring the organization of this one primary retinal target, the dLGN, with the purpose of informing questions about the functional organization of this region. The dLGN is known not only as a relay point between the vertebrate eye and the cortex; the nucleus also selects, modifies, and processes information from and to many other parts of the brain (for review see Jones, 2007). In addition, the dLGN is highly organized, keeping distinct the parallel lines of processing that run from the eye to primary and secondary visual regions– pathways comprising neurons with different morphological, physiological, and chemical properties (Anderson, 2009; Jones, 2007, for review). In the primate, these pathways lay out in six easily cytoarchitecturally-distinguishable layers, each receiving inputs from a specific set of retinal ganglion cells (RGC), magnocellular, parvocellular, or koniocellular. In addition, each layer receives input from a specific eye, and retinotopically maps the world based on the properties of the RGCs from which it samples. Similarly in the cat, a representative carnivorous mammal, the dLGN has five layers which also receive inputs from different classes of RGCs and are also organized in a retinotopic manner (Murray et al., 2008; Jones, 2007, for review).

In some ways, the dLGN is laid out similarly. Physiological evidence shows that the lines of projection falling on the dLGN from the retina create a topographic map in the rat as it does in other mammals, and that as in the cat, the projection lines from the ipsilateral eye in general run obliquely to those from the contralateral eye (Reese and Jeffrey, 1983). Additionally, projections to the dLGN from the rat optic tectum, another major retinal target, also show parallels to those of the cat and macaque (Reese, 1984).

Yet despite these physiological similarities, the detailed anatomy appears to be quite different. The rat dLGN contains a homogenous-looking cell population which has been farther divided by some RGC eye-of-origin information (Reese and Cowey, 1983), general RGC cell-type distinctions (Fukuda, 1977; Hickey and Spear, 1976), organization of collicular input (Reese, 1984), and some retinotopic projection-line information (Reese, 1988). Such studies have led to the theory that the rat dLGN contains one smaller amorphous region of ipsilateral RGC input within a much larger, contralateral-recipient structure, bordered by an 'outer shell' of contralateral input. It is generally accepted that these rat ipsi- and contra-regions are segregated (for review, see Guido et al., 2006) as is known in other mammals (Hubel and Weisel, 1961), and that there is no additional anatomical substructure within these general eye-specific zones.

There have been some suggestions, however, that this simple model may not properly describe the rat dLGN. For example, one study concluded that the rat may have regions of intermixed eye-recipient zones instead of completely segregated ipsilateral and contralateral regions (Grieve, 2005). In addition, the distribution of some interneuron cell types seems to vary within the dLGN, suggesting possible functional subregions (Gabbott and Bacon, 1994). Besides the studies suggesting 'hidden lamination' in rats (Reese, 1988; Martin, 1986), others have since postulated the existence of lamination in other rodents. For example, genetic studies have found classes of motion-selective RGCs projecting to layers in the mouse dLGN (Huberman et al.,2008; Huberman et al., 2009). This evidence led us to wonder about detailed lamination or other organization in the rat dLGN as well.

In the current study, we explored the existence of anatomically-based subregions in the rat dLGN, to investigate whether the rat possesses subregional special-

ization analogous to those in more traditionally studied visual mammals. Detailed anatomical models of the rat dLGN will be increasingly useful as the rat becomes more ubiquitous in vision research. Our first goal was to describe the retinorecipient region in general – specifically its approximate volume and size relationships to other landmarks such as the optic tectum and the ventral lateral geniculate (vLGN). To do this, we binocularly injected fluorescently-tagged cholera toxin B subunit, an efficient anterograde RGC tracer, to visualize retinal termination zones in the rat dLGN. We were then able to map and model the ipsilateral and contralateral contributions to the region. Secondly, we investigated the question of binocularity within the dLGN. To do this, we used the ratios of fluorescent tracers in RGC termination zones to ask whether there might exist regions that contain retinal termini from both eyes, from which relay cells might sample. And finally, we were interested in whether the shapes, areas and densities of cell bodies within the dLGN might give us any farther evidence for 'hidden lamination' in the rat. Based on these analyses, we address the question of whether or not cytoarchitecturally-distinct sublaminae might exist in the rat as they do in cat and monkey.

2.3 Methods

2.3.1 Subjects

Eight normal naive adult male Long Evans rats (Harlan Laboratories, Inc.) were used in this study. Half were later injected binocularly; these four rats were aged 3-4 months and weighed between 370 and 440 grams. The four subjects that were later injected monocularly were aged 6-7 months and weighed between 490 and 670 grams. All subjects were maintained on a 12-hr light/dark cycle with free access to food and water. All procedures were supervised and approved by the Institutional Care and Use Committee at the University of California, San Diego.

2.3.2 Intra-ocular injections

The B subunit of the cholera toxin complex (CTB) has been shown to be a highly-sensitive anterograde tracer for RGCs (Matteau et al., 2003; Rainer et al., 1996; Angelucci et al., 1996), and therefore the preferred tracer for this study. Rats were first anesthetized with 2-5% isoflurane mixed with oxygen at a flow rate of one liter per min, using an isoflurane vaporizer (Smiths Medical, Dublin, OH.) While maintained at the appropriate level of anesthesia, subjects were subcutaneously injected with buprenorphine (0.06 mg/kg rat weight.) Subjects then received, via syringe, 5-6 2μl injections of either unconjugated CTB in one eye, or fluorophor-conjugated CTB in both eyes. The monocular injections were administered into the vitreous chamber of the left eye only, and comprised a 1% CTB solution (List Biological Laboratories, Inc., Campbell, CA) mixed with 2% dimethyl sulfoxide (DMSO) diluted in sterile water. In the fluorescent case, rats were injected with two different fluorophor CTB conjugations, one in the vitreous chamber of each eye. We used a 1mg/ml dilution of Alexa Fluor 488-conjugated CTB (Molecular Probes Inc., Eugene, OR) in PBS injected in the left eye, and a similar dilution of Alexa Fluor 594-conjugated CTB in the right eye (Molecular Probes Inc., Eugene, OR).

During the post-injection survival period, subjects received a minimum of twice-daily buprenorpnine injections for 2-3 days, with injections continuing as needed.

2.3.3 Perfusion and histology

Five to seven days post-injection, all rats were euthanized with an overdose of isofluorane, and perfused transcardially with 0.1M phosphate-buffered saline (PBS; pH 7.4) followed by 4% paraformaldehyde in PBS. After removal, brains were further fixed in 4% paraformaldehyde for at least three days, after which they were then soaked in a 30% sucrose PBS buffer solution for cryoprotection prior to slicing. Brains were sliced on a freezing microtome (Microm International GmbH, Waldorf, Germany); non-conjugated monocularly-injected rats were sliced at 30μm in one of the three planes, and binocular rats were sliced at 25μm coronally.

Non-fluorescent tissue samples were processed according to the method described by Angelucci et al. (1996) and Matteau et al. (2003). In the case of this study, the antibodies for visualizing the cholera toxin stain showed appropriate morphology and distribution of RGCs as demonstrated in these previous publications.

In summary, tissue was rinsed in phosphate buffered saline, and then incubated and rotated at 4° Celsius overnight in a primary antibody solution of 0.1% Triton X-100, 5% normal rabbit serum, and a 1:1000-1:2000 dilution of biotinylated goat anti-rabbit CTB (List Biological Laboratories, Inc., Campbell, CA, cat #103B) in phosphate buffered saline. After rinsing again with phosphate buffered saline, tissue was then incubated and slowly rotated for one hour at room temperature in the secondary antibody solution consisting of a 1:1000 dilution of Vectastain biotinylated IgG (Vector Labs, Burlingame, CA, cat #PK-4005) with 0.3% Triton X-100 in phosphate buffered saline. Finally, after a third set of rinses, tissue was incubated in a tertiary antibody solution made using the Vectastain ABC kit ElitePK-6100 kit (Vector Labs, Burlingame, CA). Tissue was incubated in a complexed avidin-biotin-peroxidase solution diluted to 1:1000 in phosphate buffered saline with 0.3% Triton X-100 and additional 2% NaCl. To visualize the CTB, the tissue was rinsed in buffer and soaked in a 1:3000 hydrogen peroxide phosphate buffer solution with 0.125 mg/ml Diaminobenzidine (DAB) for approximately 1 minute, or until cells reacted. Tissue was rinsed, mounted on gel-coated slides (Thermo Fisher Scientific Inc., Pittsburgh, PA), enhanced with 4% osmium, and coverslipped. One series from each brain was reacted with DAB alone, one series was counterstained with Geimsa as well as DAB, and another series was Nissl stained for cell bodies.

Fluorescent samples were also separated into four series and mounted with Prolong Gold anti-fade reagent medium (Molecular Probes Inc., Eugene, OR) on charged slides (Thermo Fisher Scientific Inc., Pittsburgh, PA) before coverslipping. After the initial round of imaging, slides were soaked to remove the coverslip, photobleached, and stained with NeuroTrace 500/525 nm green fluorescent nissl stain (Molecular Probes Inc., Eugene, OR) before re-imaging.

2.3.4 Imaging

The non-fluorescent DAB/Geimsa series was scanned using Aperio Scanscope XT digital slide scanner (Aperio Technologies Inc., Vista, CA; Burnham Institute, La Jolla, CA) at 20x resolution, aligned using ImageJ software (Abramoff et al., 2004), and analyzed using several MATLAB modules (2008a-2010a, The MathWorks, Natick, MA). Fluorescent samples were imaged twice (once to capture retinal afferents, once to capture nissl bodies) on the NanoZoomer 2.0 HT digital slide scanner (Hamamatsu Photonics, Japan). Slides were imaged at 20x using the fluorescent cube (DAPI/Fluorescein isothiocyanate/TexasRed). To confirm complete CTB staining of projecting ganglion cells, we examined all sections of the dLGN and as many sections of the optic tectum as were available, to ascertain uniform staining.

2.3.5 DLGN tracing and 3D reconstructions

After photographing, we hand-traced subregions of the dLGN based on RGC termini projection zones from the two eyes using The Rat Brain Stereotaxic Atlas (Paxinos and Watson, 1998, fourth edition) for initial nuclei identification. Retinal ganglion cell axons and their terminals were traced at high resolution using the software Neurolucida (MBF Biosciences, Inc., Williston, VT).

When tracing images, outlines were made delineating: a) the entire dLGN, tracing the outer edge of both ipsilateral and contralateral termini, b) ipsilateral subregions, or contiguous regions containing high densities of puncta from the ipsilateral RGC termini, c) and the 'holes' in the contralateral zones, or contiguous regions within the dLGN lacking high densities of puncta originating from the contralateral retina.

We then used these tracings to make 3D reconstructions of these regions, also using Neurolucida software.

2.3.6 Volume calculation

Using the traced outlines around the retinal projection zones, we were able to calculate the volume of the retinorecipient dLGN as well as that of the ventral

lateral geniculate nucleus (vLGN) and optic tectum (optic tectum), two other major RGC targets. We traced these regions using Neurolucida in the same manner as we did the dLGN, and then used a formula postulated by Sackett et al. (1989) and used by Najdzion et al. (2009) to calculate their estimated volumes. Here, the total volume of the structure (V_0) is estimated by the sum of the sub-volumes throughout the region of interest (V_n). Therefore: $V_0 = \sum_V n$. Each sub-volume was calculated using the formula, where

$$a_n = area\ of\ one\ slice\ through\ the\ region\ of\ interest$$

$$V_n = (\frac{distance\ between\ sections}{3}) \times a_n + a_{n+1} + \sqrt{a_n} \times a_n$$

The sub-volumes of the extreme sections (end poles) were estimated by the formula:

$$V_n = (\frac{distance\ between\ sections}{3}) \times a_n$$

2.3.7 Analysis of the segregation of RGC termination zones

To determine the prospective overlap of CTB-stained terminals in retinal projection zones, we used analyses inspired by Torborg and Feller (2004) along with MATLAB code created specifically for the purpose. To do this, we masked the original fluorescent binocularly-injected images using the outlines made in Neurolucida. We first corrected for bleedthrough fluorescence found from the green channel into the red channel, by locating all pixels containing 95% of the maximum green staining and setting their red intensities at those locations to zero. We then subtracted the background from these masked images – a threshold chosen from each slice that when visually inspected, spared termini while removing fibers of passage. After thresholding, we were then able to calculate the 'R value' for each pixel in the masked images (Torborg and Feller, 2004), where

$$R = log(\frac{intensity\ of\ ipsilateral\ staining\ of\ pixel}{intensity\ of\ contralateral\ staining\ of\ pixel})$$

We calculated the R-values at multiple different smoothing diameters, made using a circular averaging filter in MATLAB.

2.3.8 Stereoptics and cytoarchitectural analysis

To more closely examine the cellular organization of the dLGN throughout the nucleus as well as for distinct subregions (as determined by the Neurolucida tracing described above), we performed cell size and density calculations using CellProfiler (cellprofiler.org; Carpenter et al., 2006), an open-source MATLAB code. We used this code to identify and outline prospective cells, and to calculate the following properties: orientation, compactness, radial distribution, distance to closest neighbor, angle between neighbors, area, eccentricity, solidity, and compactness.

In summary: orientation is the angle (in degrees ranging from -90 to 90) between the x-axis of the cell and the major axis of the ellipse that has the same second-moment as the cell. Compactness is defined as the variance of the distance of the cell's pixels from its center, divided by its area. Radial distribution is a measure of the intensity distribution from each cell's center to its boundary. Distance to closest neighbor is the distance in pixels to a cell's nearest neighboring cell. Angle between neighbors is the angle formed between the cell's center and its first and second closest neighbors. Area is the number of pixels falling within the identified cell. Eccentricity is defined as the ratio of the distance between the foci of the ellipse that has the same second-moment as the cell and the cell's major axis length. Solidity is the proportion of the pixels in the convex hull that are also in the region, where the convex hull is the smallest convex polygon that fits around all the pixels in the cell. And finally, compactness is the variance of the distance of the object's pixels from its center, divided by its area.

2.4 Results

2.4.1 Imaging termini and tracing nuclei

For the fluorescent samples, we coronally sliced each perfused brain into 25μm thick sections and imaged every fourth section using a Nanozoomer 2.0 HT (see methods). All inputs from the left eye fluoresced green (488 nm), and all inputs from the right eye fluoresced red (594 nm). Upon inspection of all dLGN and optic tectum sections imaged, we noted that although uneven in places, these

primary retinal targets showed staining throughout three of the four rats, 392, 395, and 397. From this, we induced complete filling, and these rats were included in all analyses. When examining the fourth subject however, we noticed unstained locations in retinal targets that, were the retinal injections successful in completely filling all ganglion cells, should have contained stained termini. While we were still able to outline the dLGN and its subregions by eye, it did not pass our criteria for a complete injection, and therefore this subject was excluded from the input segregation analysis.

Figure 2.1A shows an example photograph obtained from a representative coronal section. The top image is of both dLGN from the rat 395, one of four completely filled binocularly-injected subjects. The bottom zoomed-in image is that of the right dLGN in this same rat. In these three binocular subjects, we also observed stained retinal termini throughout other known major retinorecipient regions such as the optic tectum, here shown in Figure 2.1B (top) in rat 395. Figure 2.1B (bottom) shows, in contrast, an example image of the optic tectum taken from the monocularly-injected rat 144. All monocularly-injected light-imaged subjects were sliced coronally at 30μm, counter-stained with Geimsa, and photographed using the Aperio Scanscope (see methods).

After imaging both the monocular and binocular brains, we hand-traced around regions with dense RGC termini puncta. In Figure 2.1C, example tracings of the whole-dLGN (top) and zoomed-in dLGN subregions (bottom) show the relationship between the termini and detailed tracings.

In this manner we obtained complete traced series of every fourth section through the lateral geniculate nucleus (LGN) and surrounding brain for 4 binocularly injected samples and 3 monocularly injected non-fluorescent samples. On the basis of these data, we determined the volume of the dLGN relative to other regions (table 1), the structure of ipsilateral subdomains in the dLGN (Figures 2.2-2.5), the extent of overlap of the ipsilateral and contralateral projections to the dLGN (Figures 2.6-2.10), and various cell body statistics within these eye-of-origin defined subdomains (Figures 2.11-2.13).

Figure 2.1: Example images of raw data collected from NanoZoomer and Aperio Scanscope, over which all regions were traced.

(facing page)

Binocular subjects were injected with Alexa-Fleur 488nm-conjegated CTB (green) in the left eye and AlexaFleur 594nm-conjugated CTB (red) in the right eye. Non-fluorescent subjects were injected with non-conjugated CTB in the left eye only. *A:* One sample image showing both dLGN of the coronally-sliced rat 395 (top), one of four binocularly-injected subjects. Bottom: from the same rat, a zoomed-in image of the right dLGN. *B:* Examples of photographs of the optic tectum in coronally sliced rats; the top image was taken from the binocular rat 395, the bottom image from rat 121, a geimsa counterstained monocular CTB-injected brain. *C:* Example image of the tracing done bilaterally on every fourth section of each of the brain. The subcortex, as well as the outline of the entire dLGN, the holes in the projections from the contralateral eye, and the projections from the ipsilateral eye were all separately traced. On the right is a zoomed-in image of this tracing to show the relationship between the detailed RGC termini and subregion tracings. The subcortex is outlined here in green, the dLGN in red, holes in the contralateral projection zones in magenta, and ipsilateral projection zones in cyan.

A.

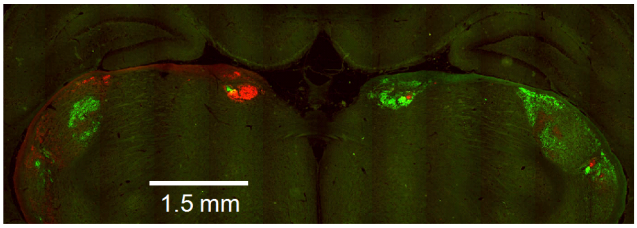

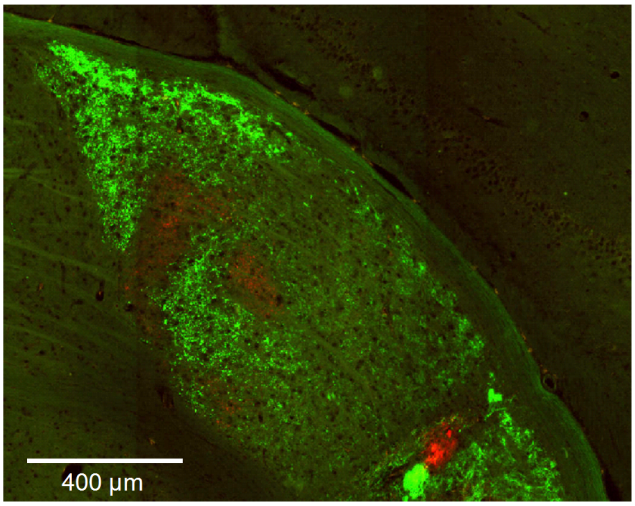

B.

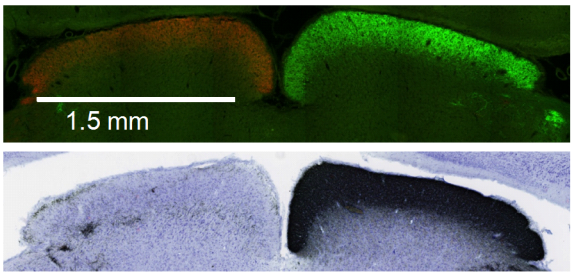

C.

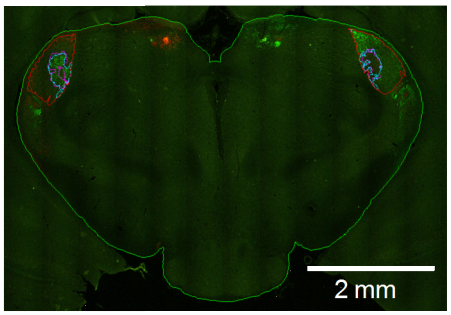

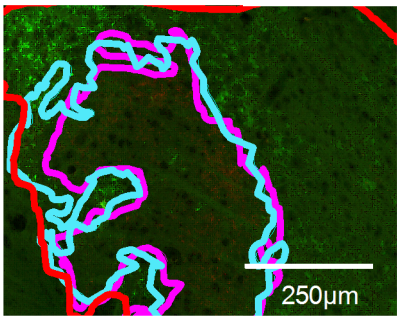

2.4.2 Volumes

Using the Sackett calculation described in the methods section, we found the volumes of the dLGN, vLGN (a combination of the vLGN and intergeniculate leaflet,) and the optic tectum (see Table 1.) We found that, on average, one dLGN has a volume of $1.58mm^3(\pm 0.094mm^3$, $n = 9$ dLGN nuclei from 7 rats). This is $70.0\%(\pm 3.0\%$, $n = 3)$ of the total RGC-recipient geniculate volume (vLGN and dLGN), $40.4\%(\pm 1.0\%$, $n = 3)$ of the volume of the optic tectum. Thus the dLGN is smaller than half the volume of the retinorecipient layers of the optic tectum, but constitutes the majority of the retinorecipient zone in the thalamus.

Table 2.1: Summary of volume data collected from six binocularly-injected subjects.
Subjects 392, 395, 397, and 399 were binocularly-injected, and we were therefore able to measure both sides of the bilateral retino-recipient LGN. Subjects 144, 156 and 157 were monocularly injected, so only termini on one side of the brain was visible. Therefore only the right structures were measured. Optic tectum and vLGN/ILGN were traced completely in the monocular brains only.

subject #	left dLGN	right dLGN	left IGL/vLGN	left optic tectum
rat392	1.63mm^3	1.59mm^3	--	--
rat395	1.76mm^3	1.56mm^3	--	--
rat397	1.55mm^3	1.59mm^3	--	--
rat399	1.66mm^3	1.63mm^3	--	--
rat156	1.53mm^3	--	3.70mm^3	0.552mm^3
rat157	1.46mm^3	--	3.71mm^3	0.687mm^3
rat144	1.42mm^3	--	3.51mm^3	0.652mm^3

2.4.3 Putative ipsilateral subdomains within the dLGN

We then looked at the dLGN in more detail, analyzing the regions containing ipsilateral projections separately from those contralateral-recipient regions. Again, Figure 2.1C shows an example image of the tracing done bilaterally on every fourth section of each binocularly-injected brain (top), along with a blown-up region of RGC termini to show tracing in detail (bottom). With these ipsilateral and contralateral tracings, we made three-dimensional reconstructions of the dLGN from the four binocularly-injected subjects. Figure 2.2A shows the 3D reconstruction of the ipsilateral regions within the left dLGN (left) and the right dLGN (right) from one brain (rat 395, as a representative example). We then were able to see geographically-distinct subregions of ipsilateral termini, which we have colored separately in Figure 2.2B. To separate out subregions, we looked for disconnected groupings of ipsilateral projections within the dLGN. Because we traced from every fourth section, in some cases we estimated where these geographic divisions were located.

In this way, we subdivided the ipsilateral projection zones within all brains, on both the left hemisphere dLGN (Figure 2.3) and right hemisphere dLGN (Figure 2.4) of each subject. We found, in general, three categories of ipsilateral subregions: a dorsal-medial, a ventral-rostral, and a larger central region. While the number of these subregions (see Figure 2.5 for summary) and their exact locations varied from animal to animal and even between hemispheres in the same animal (see Figures 2.3 and 2.4), the approximate locations of these ipsilateral subregions remained generally consistent. From these data we conclude that the dLGN of the pigmented rat typically contains multiple ipsilateral projection zones, and not one single zone as described previously.

Figure 2.2: 3D reconstructions of ipsilateral subregions within the dLGN, as made by tracing and aligning sections throughout each brain.

(facing page)

A: An example of all reconstructed ipsilateral-recipient regions within the left (left) and right dLGN (right) of rat 395, a representative binocularly-injected subject. Here, regions of ipsilateral termination are colored green inside of the red-outlined dLGN outer boundary, to show their locations within the nucleus. The nissl-stained images above are for dLGN contextual reference within a slice. *B:* The same dLGN outlines as in *A*, but here they are separated into geographically distinct subregions, pseudo-colored for ease of visualization.

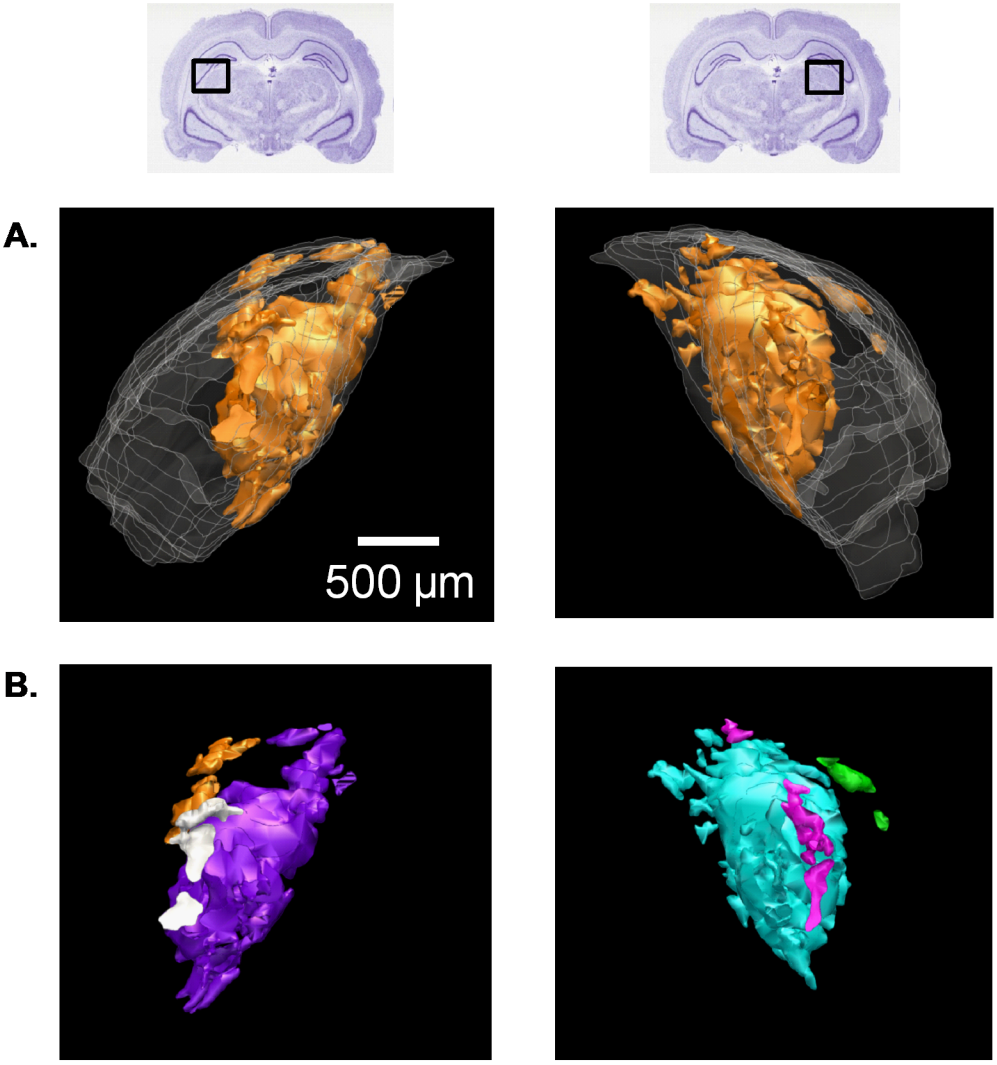
A.
500 µm
B.

Figure 2.3: 3D reconstructions of the left dLGN from the four rats studied, colored to show the separation between distinct ipsilateral-recipient subregions.

(facing page)

Each reconstruction is shown from three different vantage points: the top, front, and side view. The vantage point is illustrated at the bottom, with the dLGN position marked by a black square on a whole-brain icon.

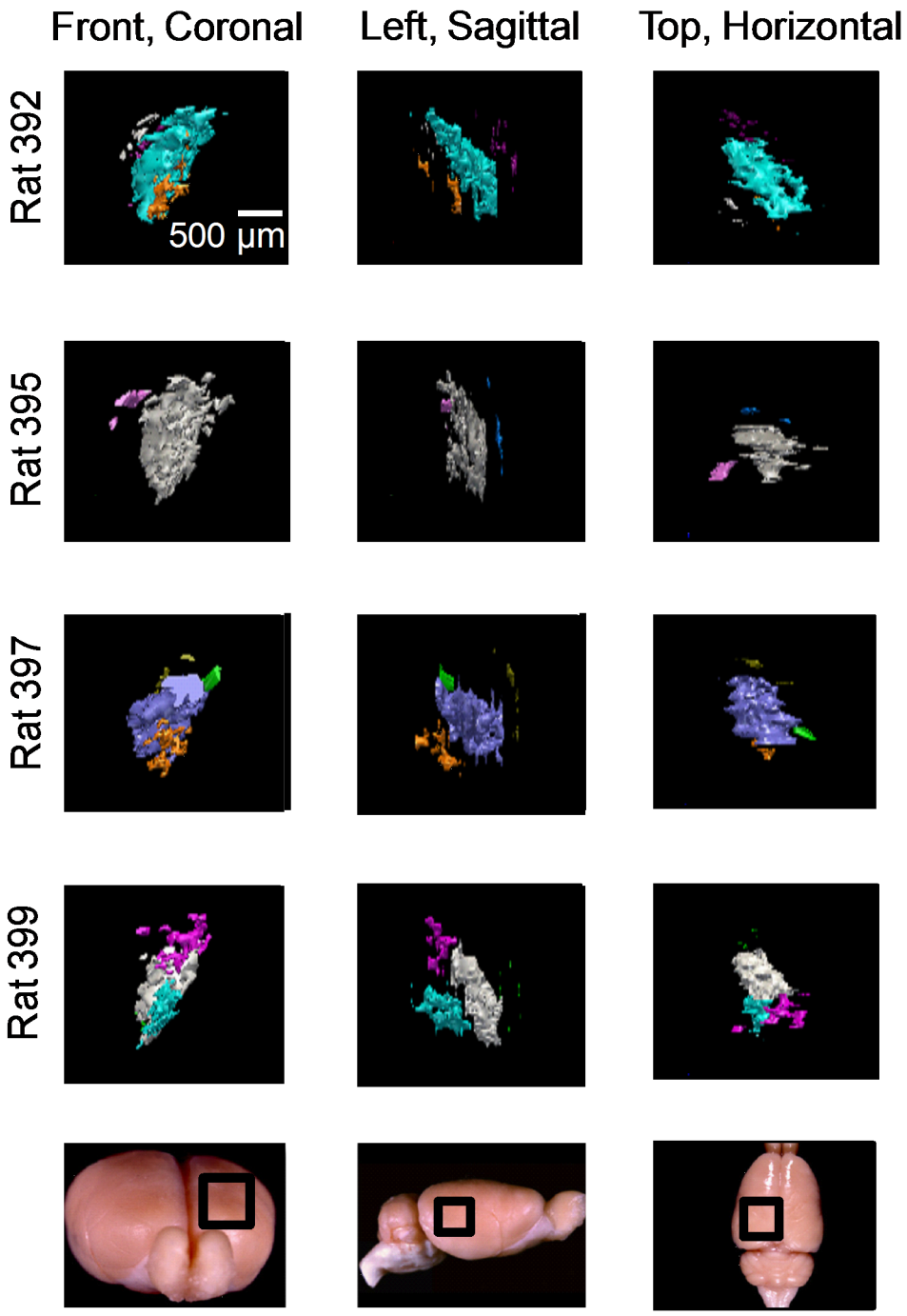
Front, Coronal
Left, Sagittal
Top, Horizontal
Rat 392
Rat 395
Rat 397
Rat 399
500 µm

Figure 2.4: 3D reconstructions of the right dLGN from the four rats studied, colored to show the separation between distinct ipsilateral-recipient subregions.

(facing page)

Each reconstruction is shown from three different vantage points: the top, front, and side view. The vantage point is illustrated at the bottom, with the dLGN position marked by a black square on a whole-brain icon.

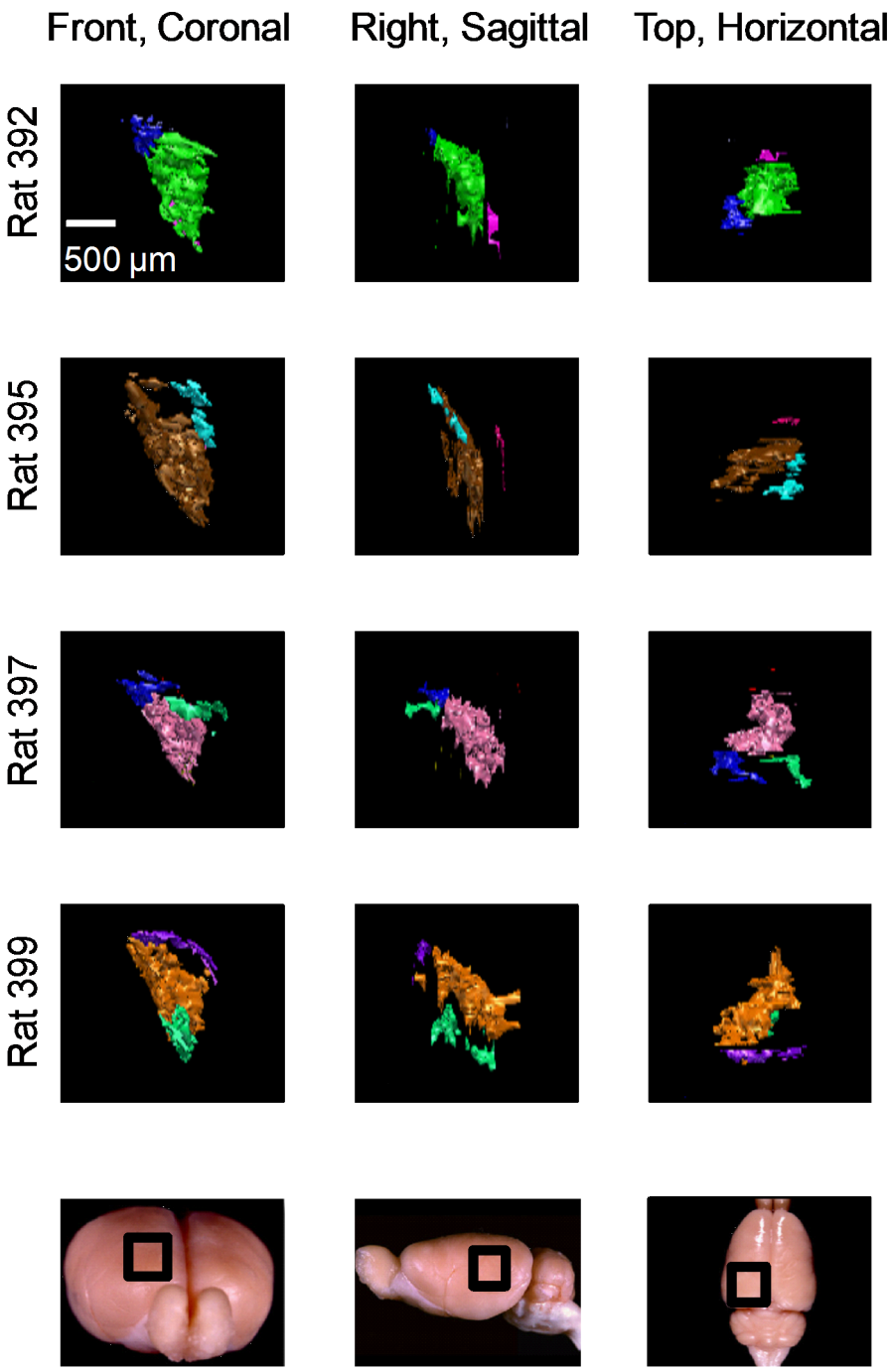
Front, Coronal
Right, Sagittal
Top, Horizontal
Rat 392
Rat 395
Rat 397
Rat 399
500 µm

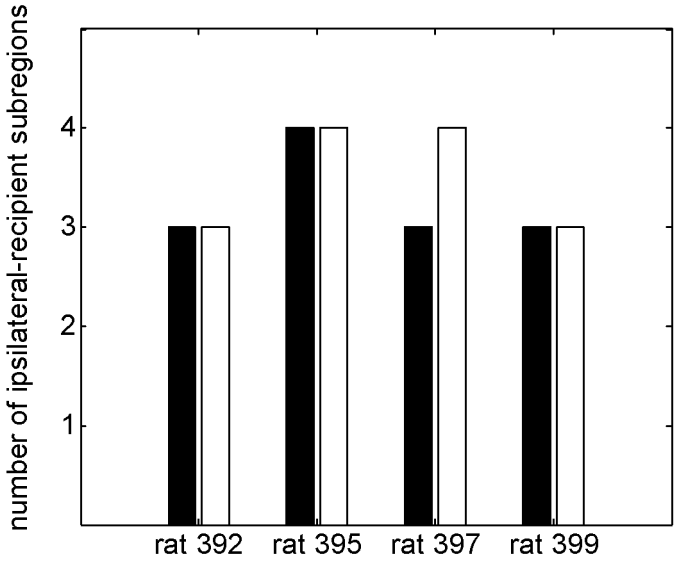

Figure 2.5: The number of distinct ipsilateral-recipient regions in the dLGN, as observed in the four binocularly-injected rats in this study.
These regions were identified by eye from 3D reconstructions assembled from outlines traced around RGC termini. Black bars represent the number of subregions in the left dLGN, and white bars represent subregions in the right dLGN.

2.4.4 Spatial segregation of retinal termination zones within the dLGN

In addition to visually examining the subregions in the dLGN, we also quantified the degree of overlap of the termini emanating from the two eyes. Considering that binocular responses have been reported in the literature (Greive, 2005), it is of interest to know if relay cells themselves could theoretically sample from both eyes. To address this question, we used information about the intensity and location of fluorescence to analyze the segregation of termini, based on a method introduced by Torborg et al. (2008). In their study, they measured binocularity with the ratio R, or the log of the ipsilateral intensity at an image location over the the contralateral intensity at that same location (see methods). We calculated this R-value at different smoothing diameters for all pixels throughout the three binocular subjects, in order to simulate prospective sampling regions of relay neurons.

To examine the degree of binocularity, we first determined an R-value criteria for calling locations in an image 'binocular', or in other words, locations containing a substantive amount of fluorescence from both eyes. While we cannot make a judgement from these methods about the absolute fluorescence and how much is a 'substantial' binocular input to a region, we did suppose that any ratio of input from one eye to the other eye that exceeded 100/1 should be considered monocular. Therefore, we chose the corresponding R-values of 2 and -2 as our cut-off for binocularity. In all sampling-size conditions, locations with an R-value of -2 or smaller were deemed monocular and contralateral, and those pixels with R-values of 2 or greater were monocular and ipsilateral. Figure 2.6A shows a summary of R-values or all pixels in the three fluorophor-injected rats included in this study. Because there are far fewer binocular pixels than monocular, we farther examine the binocular pixels by zooming in to the central R-value region in Figure 2.6B. In Figure 2.6B, the values between -2 and 2 (demarcated by dashed vertical lines in the first panel) were considered binocular. As expected, as the sampling diameter increased, the percentage of pixels classified as binocular also increased for all rats (2.6B). We also noted that there were several peaks in the binocular region

– one large peak close to the cutoff for monocular and contralateral, one centered closer to zero, and in some rats, a smaller peak of mostly-ipsilateral staining.

Due to the weak staining that we sometimes observed in the red channel of several of the rats, we wondered if these peaks seen in the R-value distributions could be caused by differences in staining between the red and green dyes. To look more closely at this question, we separated out R-values by hemisphere (Figure 2.7) and examined the R-distributions where red was the contralateral dye (Figure 2.7, top) separately from when green was the contralateral dye (Figure 2.7, bottom).

Besides the proportion of binocular pixels across subjects, we were also interested in looking at the substructure of the binocular summary data. Figure 2.8 shows data from rat 395 as a representative example. In Figure 2.8, we show the absolute input strengths for all pixels in the image (Figure 2.8A, left), as compared with pixels classified as binocular according to R-value criteria (Figure 2.8A, right). It is clear that once pixels with R-values greater than 2 or less than -2 are removed, the remaining binocular pixels falling along the line x=y, are fewer. As we increase the sampling diameter (Figure 2.8B), we notice that the number of binocular pixels increases as expected, for the number of pixels receiving input from one eye only decreases as do the number of pixels receiving no input from either eye. In Figure 2.8, this increase in the number of binocular pixels is illustrated with increasing warmth in the 2D histogram. In addition, we noted that even the pixels deemed binocular could be farther described as being either contra-dominant or ipsi-dominant; this structure can be seen within the binocular pixels in Figure 2.8B.

Figure 2.6: Population of R-values for every dLGN pixel in the four binocularly-injected subjects.

(facing page)

For each binocularly-injected rat examined, we calculated the 'R-value', or the ratio of the log of the ipsilateral intensity at a given pixel to the contralateral intensity at that same pixel (Torborg et al. 2008, see methods). This line plot shows the population of all R-values for every dLGN pixel in the three rats studied here. R-value is shown on the x-axis and the proportion of all pixels in the dLGN that shares that R-value is on the y-axis. The red line represents data from rat 392, the green line from rat 395, and the blue line from 397. For each subplot, we calculated R-values based on images that had been smoothed using a disc filter of increasing diameter: 1μm, 5μm, 10μm, and finally 20μm. Dashed lines in first panel show cutoff points for binocular classification. In this experiment, all pixels with R-values between -2 and 2 were deemed binocular.

A.

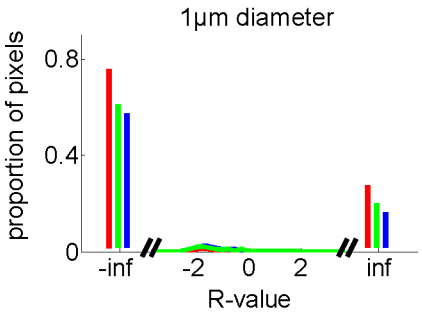
1µm diameter
proportion of pixels
0.8
0.4
0
-inf
-2
0
2
inf
R-value

B.

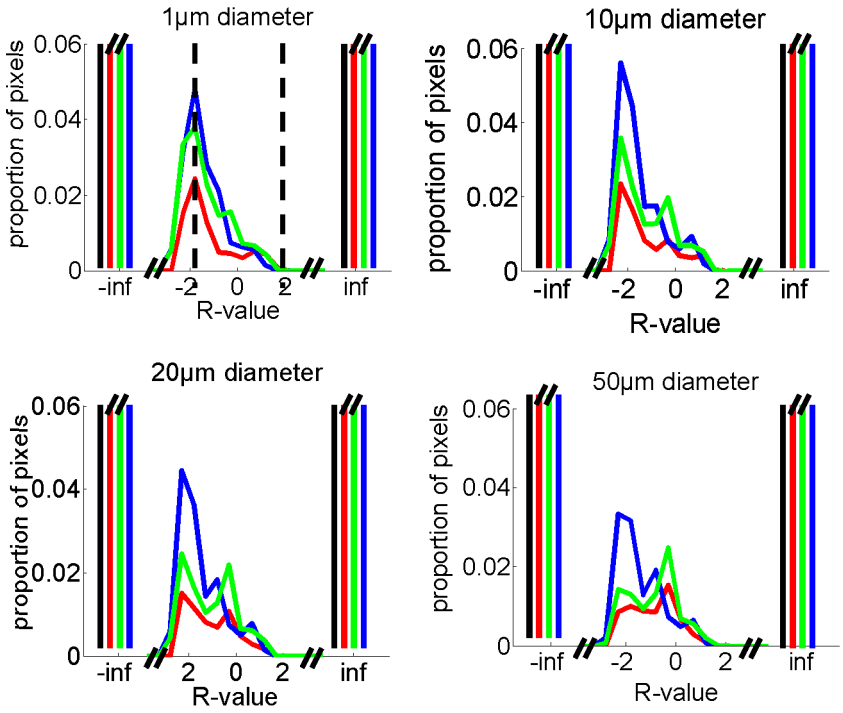
1µm diameter
10µm diameter
20µm diameter
50µm diameter
proportion of pixels
0.06
0.04
0.02
0
-inf
-2
0
2
inf
R-value

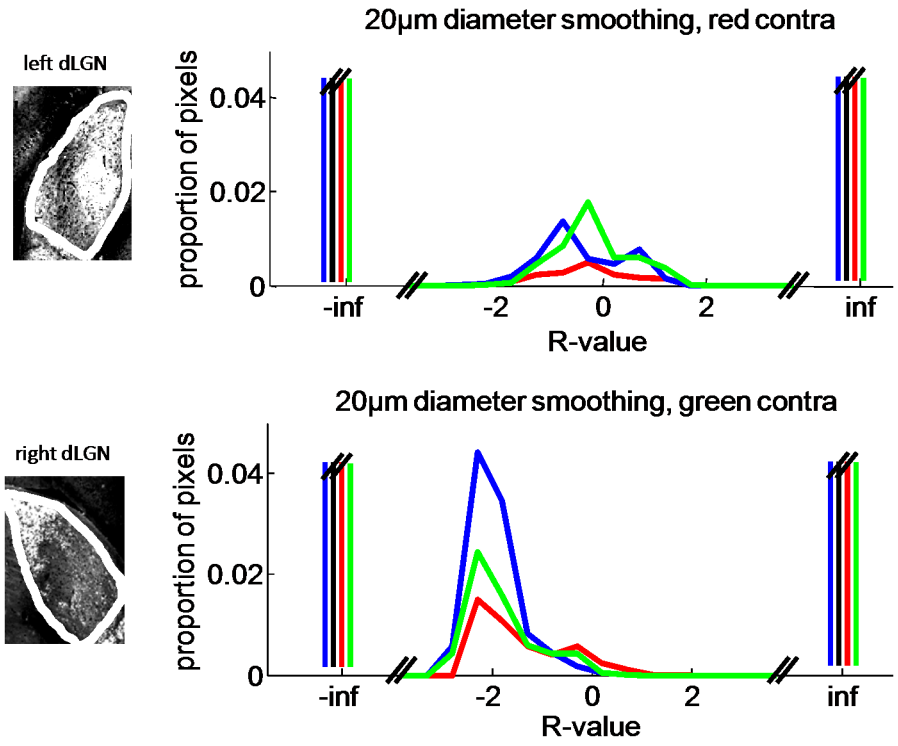

Figure 2.7: All R-values calculated throughout the four binocularly-injected subjects, as separated by hemisphere.
In this figure, data are separated out based on hemisphere – the top line plot sums across all left dLGN where contralateral termini are stained red, and the bottom line plot sums across the right dLGN, where contralateral termini are stained green. Raw images on the left are included to illustrate hemisphere. All R-values calculated throughout all four binocularly-injected subjects; the red line represents all data from 392, green from 395, and blue from 397. Again, R-values are calculated as the ratio of the log of the ipsilateral intensity at a given pixel over the log of the contralateral intensity at that same pixel (see methods).

Figure 2.8: 2D histograms showing the number of pixels with various fluorescence intensities from the ipsilateral and contralateral channels, taken from one slice from rat 395 as a representative example.

(facing page)

In all plots, values of log contra (x-axis) vs. log ipsi (y-axis) are put into bins of size 0.3 log units^2. The scale-bars indicate the number of pixels that fall into each category of values. In *A*(left), every value of log contra (x-axis) vs log ipsi (y-axis) observed in the entire image is shown. Figure 2.8A (right) only shows those pixels deemed binocular (have R-values between -2 and 2). The red box around these binocular pixels indicates the axes in Figure 2.8B. *B:* Of the binocular pixels identified in the image, all values of log contra (x-axis) and log ipsi (y-axis) are plotted. Each of the four panels displays data calculated after applying a smoothing disk filter of radii 1, 5, 10, and 20μm.

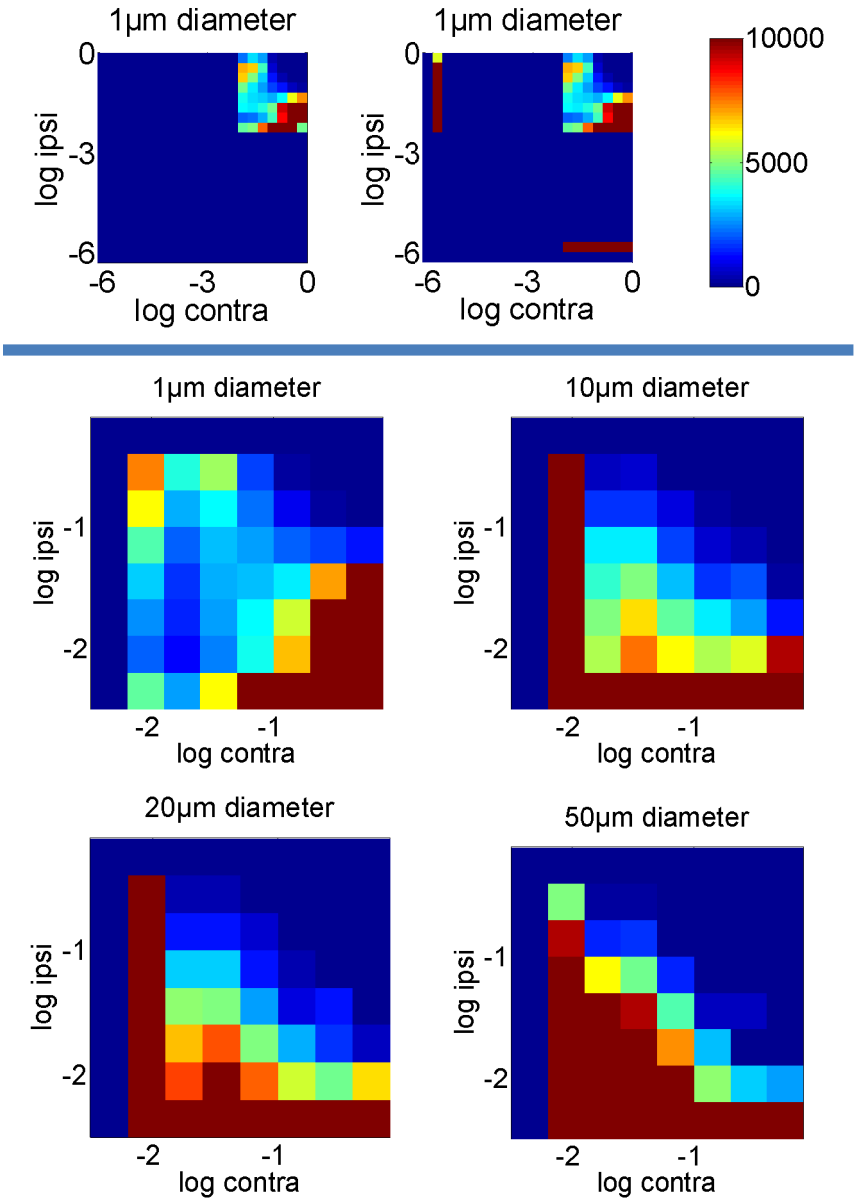
1µm diameter
1µm diameter
10000
5000
0
log ipsi
log contra
0
-3
-6
1µm diameter
10µm diameter
20µm diameter
50µm diameter
-1
-2

We then looked more closely at R-values in one sample image from rat 395, shown in Figure 2.9. Under the current R-value classification criteria, 6% of pixels in the image were binocular by a sampling diameter of 20μm (Figure 2.9B). We noted that most of these binocular pixels fell along the boundaries between ipsilateral- and contralateral- recipient regions.

We then looked at the proportion of all binocular pixels in all rats studied, at different sampling diameters ranging from 1 to 35μm (Figure 2.10.) When the images were smoothed using a disk filter of diameter equal to that of a dLGN soma (here, estimated as the 75th percentile of the major axis length of cell bodies measured, or 20μm, marked with a dashed line), on average 8% of all pixels were classified as binocular.

In summary, we find the retinal projections in the pigmented rat likely to be well-segregated with respect to eye of origin. Only a small percentage of pixels contain significant staining from both eyes when smoothed to soma-sized diameters, and these regions are largely found at the borders between ipsilateral and contralateral regions. Nevertheless, if the integration field of the relay cell is large enough, access to inputs from both eyes is possible (see discussion).

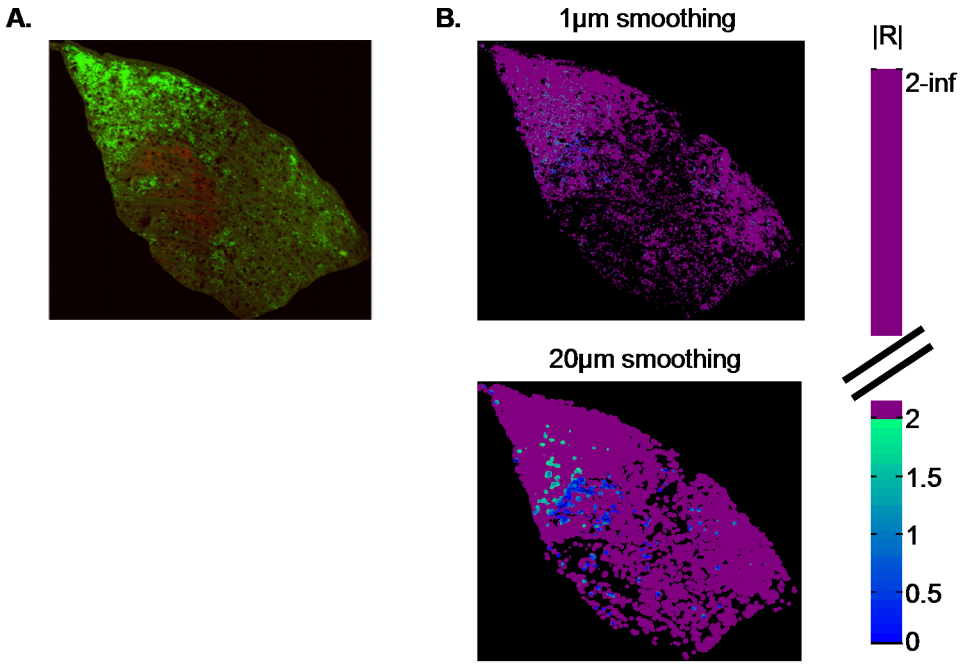

Figure 2.9: Distribution of R-values in an example coronal slice, at two smoothing diameters.
A: Raw data taken from the dLGN of one slice from rat 395, as a representative example. *B:* This same image from rat 395, at two different smoothing diameters (1μm and 20μm), where the most blue coloration indicates pixels with high-binocularity (R-values close to 0), and the most green pixels are those that have R-values close to 2, our cut-off for binocularity. Monocular pixels whose R-values are either very negative (less than 1 part in 100 from the ipsilateral eye, and therefore deemed contralateral only), or very positive (less than 1 part in 100 from the contralateral eye, and therefore deemed ipsilateral and monocular), are colored here in purple. Color bar on the right indicates the absolute value of R.

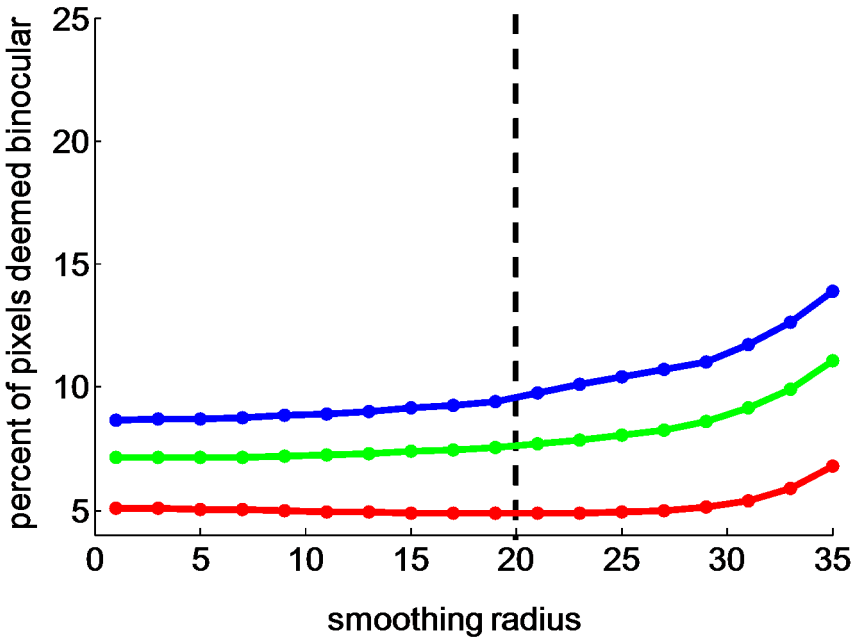

Figure 2.10: Proportion of pixels deemed binocular in all subjects at smoothing diameters between 1μm and 35μm.
A Line plot showing the proportion of pixels deemed binocular (R-values between -2 and 2) for all four subjects at smoothing diameters of 1μm through 35μm. As before, the red line represents data from rat 392, the green from rat 395, and the blue line from 397. The dashed line indicates the 75th percentile long-axis diameter for a dLGN soma.

2.4.5 Cytoarchitecture

We then used CellProfiler to identify and outline cells within the dLGN of one of our subjects, rat 395, to see if there existed any cytoarchitectural correlates of ipsilateral sublayers. We used our nissl-stained coronal images masked to the outlined ipsilateral subregions, and passed them through specialized CellProfiler analysis pipelines to calculate properties such as cell soma area, shape, orientation and density (see Methods). However, we found no evidence for spatially segregated cytoarchitectural domains in the rat dLGN. We found no significant difference in cell soma major axis orientation between cells in contralateral-recipient regions (87° ± 54°) and ipsilateral-recipient regions (9.9° ± 43.2°); t=42, p >.05. Similarly, we found no differences in mean cell area between contra (155.51μm^2 ± 57.32μm^2) and ipsi (144.00 μm^2 ± 93.65μm^2) regions; t=-20, p>.05, nor did we find any difference in distance to the closest neighboring cell (a measure of density) between contra (16.69μm ± 6.99μm) and ipsi (18.98μm ± 8.51μm) regions; t=4.03, p>.05. We also found no difference between individual ipsilateral subregions within one rat (p>.05, for pairwise comparisons).

These findings are illustrated in figures 2.11-2.13. Figure 2.11 shows eight example parameters examined for the cells throughout the dLGN. In this figure, each colored line represents data for cells within different ipsilateral-recipient regions. The overlap of all of these lines and the lack of multiple peaks shows the homogeneity of the data.

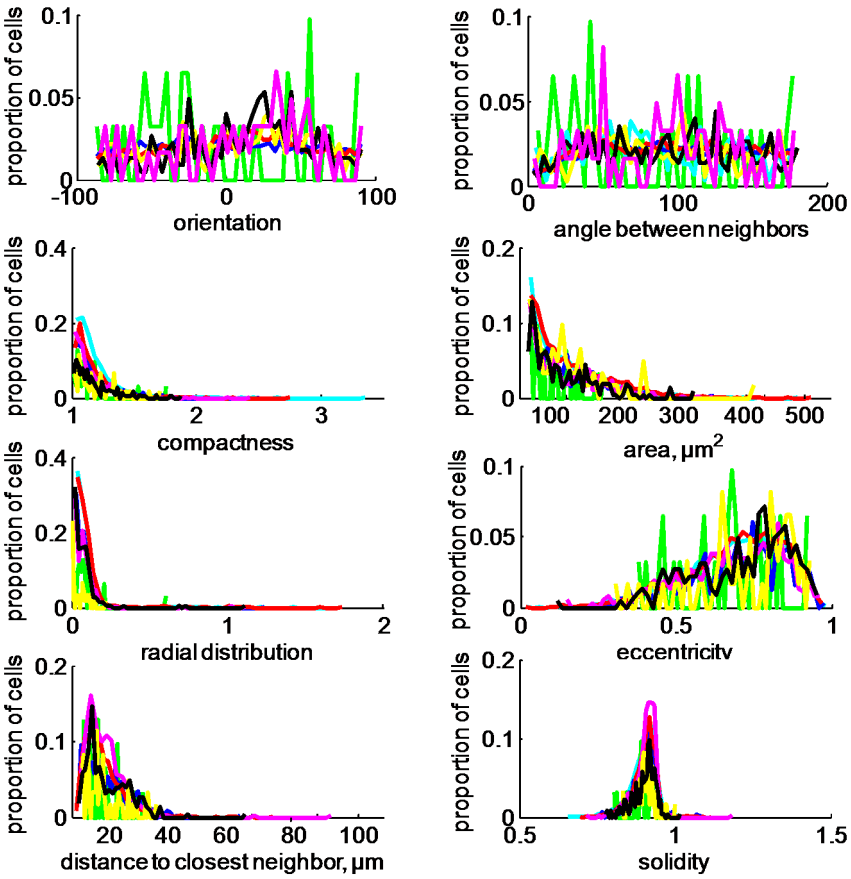

Figure 2.11: Six CellProfiler cytoarchitectural parameters extracted from rat 395 cell soma data.
For each parameter labeled on the x-axis, each colored line represents the histogram for one ipsilateral subregion isolated from the dLGN. In summary: orientation is the angle (in degrees ranging from -90 to 90) between the x-axis of the cell and the major axis of the ellipse that has the same second-moments as the cell; compactness is the variance of the distance of the cell's pixels from its center, divided by its area; radial distribution is a measure of the intensity distribution from each cell's center to its boundary; distance to closest neighbor is the distance in pixels to a cell's nearest neighboring cell; angle between neighbors is the angle formed between the cell's center and its first and second closest neighbors; area is the number of pixels in the cell; eccentricity is the ratio of the distance between the foci of the ellipse that has the same second-moments as the cell and the cell's major axis length; solidity is the proportion of the pixels in the convex hull that are also in the region, where the convex hull is the smallest convex polygon that fits around all the pixels in the cell.

Figure 2.12 illustrates four of these parameters for cells in contralateral regions (filled black circles) compared with cells within ipsilateral regions (open circles), as separated by slice throughout the brain. As shown in this figure, no differences between anterior/posterior location or eye-of-origin were seen.

Figure 2.13 shows a scatter plot of mean distance to nearest neighbor v.s. mean area for cells identified using CellProfiler methods, for rat 395. Each symbol represents cell statistics for one outlined subregion on one slice. Again, no differences were seen between different geographically-isolated subregions. These results agreed with past research suggesting no cytoarhictectural distinctions within the rat dLGN.

As a positive control for these methods, we tested this CellProfiler code on an image of the macaque to ascertain its ability to pull out cytoarchetectural distinctions in regions already known for laminar differences. Indeed, we found significant differences in cell soma properties as expected, suggesting that a lack of distinction between rat dLGN layers is due to lack of spatially segregated cytoarchitectural domains (see Appendix A).

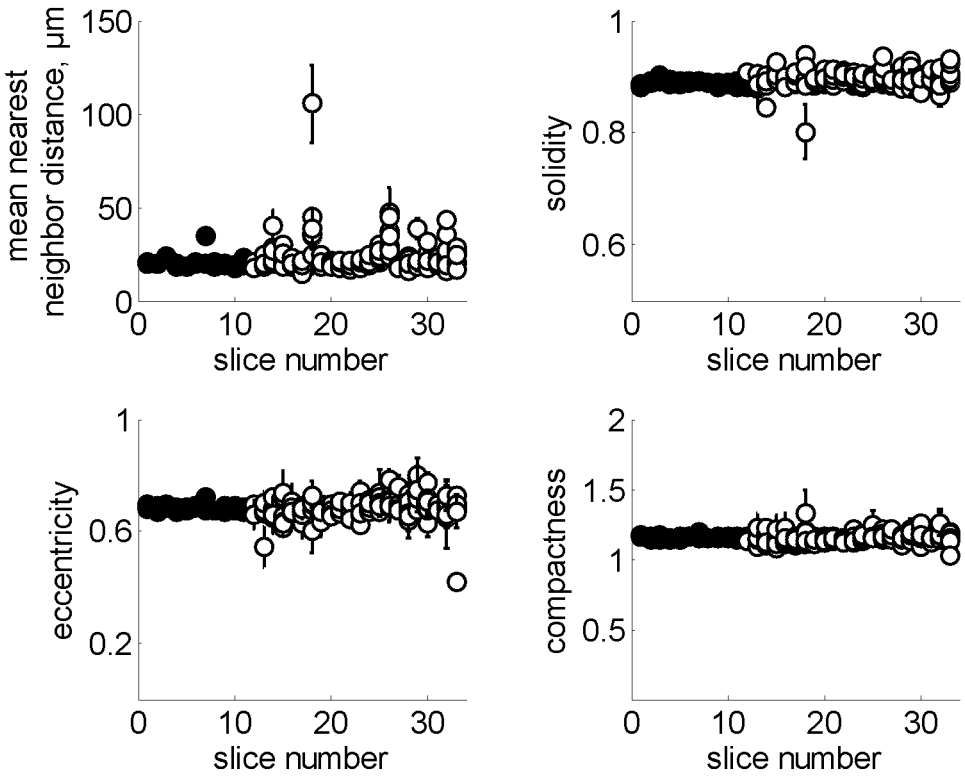

Figure 2.12: Four CellProfiler parameters extracted from rat 395 cell soma data, as grouped by slice through the dLGN.
In each of these four line plots, one CellProfiler parameter is examined, as a function of the slice along the rostral/caudal z-axis through the brain. Filled circles are means within contralateral regions on a given slice, and open circles are means within ipsilateral regions in that same slice. Error bars represent one standard deviation around the mean. In summary: distance to closest neighbor is the distance in pixels to a cell's nearest neighboring cell; eccentricity is the ratio of the distance between the foci of the ellipse that has the same second-moments as the cell and the cell's major axis length; solidity is the proportion of the pixels in the convex hull that are also in the region, where the convex hull is the smallest convex polygon that fits around all the pixels in the cell; compactness is the variance of the distance of the object's pixels from its center, divided by its area.

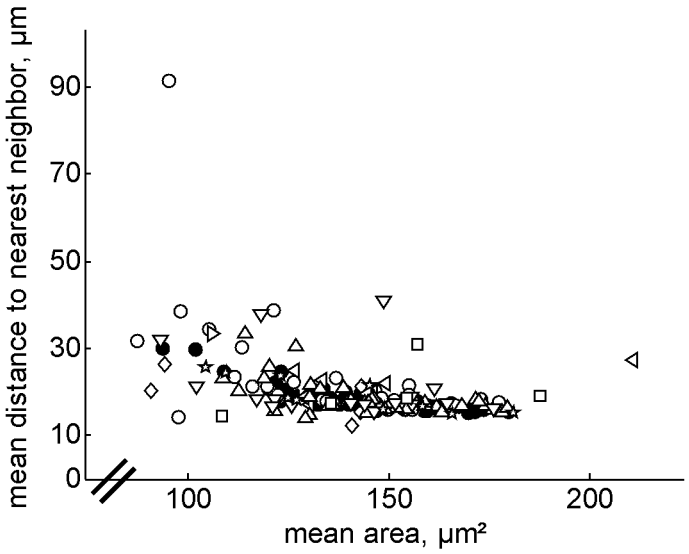

Figure 2.13: Mean distance to the nearest neighbor vs. mean area for cells within slices through different subregions.
Here, every symbol represents the mean for all cells within one region in one slice of rat 395 dLGN, where the shape represents the identity of the putative subregion. The black filled circles represent statistics from the contralateral-recipient regions. The open shapes represent the means for cells within eight ipsilateral subregions – four from the left dLGN and four from the right. Here, area is the number of pixels in the identified cell, and distance to nearest neighbor is the distance between the cell's center and the center of its nearest neighboring cell.

2.5 Discussion

Our main goal in this study was to further our understanding of the organization of the retinal termini within the pigmented rat dLGN by using anatomical techniques, in order to inspire questions about the functional organization of this nucleus. Early studies examining the rat dLGN, in contrast to the overtly layered cat and monkey nuclei, suggested some degree of 'hidden lamination' instead (Reese, 1988). It was shown that inside the contralaterally-innervated dLGN could be found one amorphous region receiving RGC termini from the ipsilateral eye. These non-distinct retinorecipient regions could be broken down farther by projecting cell type as well as retinotopy. These findings motivated the investigation into whether more could be said about the lamination of this region. To explore possible clues into this 'hidden lamination', we used CTB, a powerful RGC tracing tool, to map out termination zones in the visual thalamus. The first thing we could do after injecting the dye was to trace the locations of these termini and ask basic questions about the volumes of a few regions that they occupy. We then compared our volumetric results to those of other LGN studies in other visual species.

In their 2009 paper, Najdzion et al. compared the visual geniculate of the common shrew, the bank vole, the rabbit, and the fox. They found, in particular, that the volume of the dLGN was 0.03, 0.1, 6 and 20 mm^3, respectively. In this study, we found that the volume of the retinorecipient dLGN in the rat was an average of 1.57 mm^3, which is larger than the vole or the shrew, but less than a third the volume of the rabbit. Most of this is surely due to size – the rats in this study were about 7-10 inches long, whereas the shrew measures 5 inches, and the vole, 4.

More interesting than the absolute nuclear volumes, however, is the relationship among these volumes, and what this might say about the species studied. Najdzion et al. (2009) found that in the smaller rodent species (shrew and vole), the percentage contribution of the dLGN to the total LGN volume was about 57-58%, and considerably smaller than the rabbit (64%) or the fox (95%). Here we found the rat dLGN was approximately 70% of the retinorecipient LGN, which is larger than the percentage in the rabbit, vole and the shrew. The shrew and

the vole are both nocturnal and partially-subterranian rodents like the rat, and therefore could be considered less visually-dependent than the rabbit or the fox. It is thought that less visual species have a smaller dLGN/vLGN relative to those that depend on vision to navigate their environments (Najdzion et al., 2009).

But degree of reliance on the visual system isn't the only factor correlated with a high dLGN/vLGN quotient. In a more extensive comparison between visual thalamic volumes, Brauer et al.(1982) found that among 16 species, within a given order, those with a high level of neocorticalization also tended to have a high ratio of dLGN to vLGN volumes. This study could suggest therefore that the rat might rely more heavily on its cortex than the rabbit and the smaller rodents. In addition, Brauer found that, in general, ratios of dLGN to vLGN size were positively correlated with extent of dLGN lamination. Because we found such a high ratio of dLGN to vLGN in this study, this might be another reason to expect to find 'hidden lamination' in the rat.

After examining the nucleus as a whole, we looked farther into this possible hidden substructure within the rat dLGN. By using our tracings to make 3-D visual models of the dLGN, we found evidence of more than one ipsilateral region. There appear to be on average three or four putative subregions of ipsilateral input. These regions can be found dorsal-medially, centrally, and rostral-ventrally in general, and while the exact locations and volumes aren't well-conserved between subjects or even within hemispheres of the same brain (see Figure 2.5), this nevertheless suggests the existence of multiple ipsilateral subregions interleaved with contralateral input.

In animals with an overtly layered dLGN, each layer depicts either full or part of the visual field laid out in a retinotopic manner. To give more credence to the idea that these ipsilateral zones in the rat are indeed separate layers, one might physiologically map the receptive field spatial locations in ipsilateral subregions to find separate retinal maps. This has been done to some extent previously, however not to the fine scale necessary to reveal differences within and between subregions (Reese and Jeffrey, 1983; Reese, 1988; Reese and Cowey, 1983). Alternatively, multiple colored tracers could be injected into different regions of the visual cortex or the retina to either retrogradely or anterogradely trace the putatively separate

visual maps. If these ipsilateral regions are layers, we would see organized maps represented in each.

In addition, one could examine RGC subtypes that project throughout the dLGN (Fakuda, 1976; Huxlin and Goodchild, 1997). Several early studies found general differences in the anatomical types of RGCs that project to the 'outer shell' vs. the 'inner core' of the dLGN (Martin, 1986; see Reese, 1988). These studies found that type I (alpha) RGCs (cells with large somas and 3-6 primary branching dendrites) synapsed in the dLGN 'inner core', type II (B) cells (small somas with short dendrites) synapsed throughout the nucleus, and type III (C) RGCs (cells with smaller somas and very long dendrites) were found in the 'outer shell' only. But there are also at least a dozen functional subclasses of RGCs in the rat, each transmitting their own distinct information (Yonehara, 2009). Using techniques to trace individual functional cell types, such as molecular tags (Marc and Jones, 2002) and genetic markers (Huberman et al., 2008, 2009), we might get a better picture of the lamination within the dLGN.

Besides examining the geography of the retinal termination zones in the dLGN, we also looked at the degree of retinal input segregation to these regions. Early studies show that the mature nucleus is largely a contralateral-recipient monocular structure, surrounding but not overlapping with a small ipsilateral projection zone (Reese and Jeffrey., 1983; Reese and Cowey, 1983; Reese, 1988). A more recent study has suggested that up to 63% of the rat dLGN in fact collects and responds to direct stimuli from both eyes (Grieve, 2005). This has led to a theory that, unlike the cat and primate dLGN, some cells in the rat visual thalamus receive direct excitatory input from both eyes.

This however doesn't seem to be the case from this study presented here. By looking at the fluorescence from the RGC terminals that project to the dLGN and examining the binocular overlap of this fluorescence, it appears unlikely that dLGN cells receive input from both contralateral and ipsilateral eyes to any large extent. While it is known that dLGN relay cell dendrites span nearly the entire nucleus (Gabbott et al., 1986) making it theoretically possible for cells to sample across hundreds of microns and therefore to sample from both eyes, in cats it has been shown that relay cells only get input from RGC termini close to the soma

(Hamos et al., 1985; for review, see Sherman and Guillery, 1996). Therefore we believe that rat dLGN relay cells will similarly sample from the termini that fall close to the diameter of a cell body. When we examine dLGN binocularity at soma-sized sampling diameters of 13-20μm, we note that at the 75th percentile of cell body sizes measured (20μm), approximately 5-10% of locations within the dLGN could reach termini from both eyes. This would result in only a sixth of the number of binocular cells that Grieve noted in his study, at most (Grieve, 2005). In addition, we noted that our measured binocularly-sampling regions were located largely at the borders between ipsilateral- and contralateral-recipient regions. In contrast, there were relatively few regions with intermingled termini from both eyes resulting in a binocular region not at the border between two monocular regions.

In addition, at the sampling diameter of 20μm, most locations deemed binocular were largely-ipsilateral in staining or largely-contralateral in staining (see Figure 2.8, 20μm sampling diameter). Because we know from the literature that relay cells sample from only one to five retinal ganglion cells (Levick et al., 1972), it is possible that non-dominant-eye termini would not be sampled from. Taken together, this seems to suggest a lack of strong binocularity in the nucleus.

If indeed it is true that relay cells only sample from one eye or the other, this could mean that the dLGN's curious bilateral excitability observed by Grieve et al. (2005) is the result of another phenomenon. Instead of binocularly sampling dLGN cells, bifurcating RGC axons (Jeffrey et al.,1981; Kondo et al., 1993) or local inhibition between contralateral- and ipsilateral-recipient cells could account for the observed binocular responses (Pape, 1986). Future studies into the dLGN termination zones of these bifurcating axons would farther our knowledge of the anatomical organization in the pigmented rat.

It must be stressed that the data presented here can do no more than suggest segregation of eye inputs and therefore monocularity of dLGN relay cells; without performing farther studies to look at functional synapsing of RGC termini onto dLGN relay dendrites, we cannot know for sure from where the relay cells sample.

Finally, we used the outlines of the termination zones to examine the cell bodies within these regions, in order to ask if there are any cytoarchitectural dif-

ferences between putative subregions. From this study, the rat dLGN appears to consist of a more-or-less homogeneous group of cell somas throughout the nucleus. This however doesn't preclude the existence of morphologically, functionally, or architecturally distinct subregions. Our results simply suggest that these subregions cannot be distinguished based on the methods used here. In the mouse dLGN, a structure outwardly similar to that of the rat, it has been shown through genetic identification of several types of direction-selective RGCs that this nucleus does receive multiple laminar-specific pathways from the retina. (Huberman et al., 2008; Huberman et al., 2009; Ecker et al., 2011). In a similar fashion, it could surface that the rat dLGN receives parallel pathways as well, just not easily seen from cell-soma cytoarchitecture.

2.5.1 Low staining intensities

One possible confound to our results lies in the fact that in many cases, staining intensities of one or more of the fluorescent CTBs was weak. While CTB is known for complete filling of RGCs (Matteau et al., 2003; Rainer et al., 1996; Angelucci et al., 1996), it is also known for its frequently low-intensity fluorescence as well as fast degredation over time (Angelucci et al., 1996). While for three of the four rats staining was complete throughout the major retino-recipient zones such as the dLGN and optic tectum (suggesting filling of all RGCs), staining was uneven. In this study, the red channel occasionally stained quite weakly. This can is demonstrated in Figure 2.7, where when the contralateral region is stained red, there are more equal numbers of contralateral and ipsilateral pixels (top), whereas when the contralateral region is green, there are many more contralaterally-staining pixels (bottom).

Because of this weak staining, after subtracting background and fiber-of-passage fluorescence, we might have missed some signal from the RGCs. This could have biased our binocularity conclusions in favor of segregated eye inputs. However, at our cell-body-sized sampling diameter of 20μm we did notice notice that between 5 and 10% of the locations in the image would have access to input from both eyes. That these locations were located largely at the borders between

ipsilateral and contralateral subregions, where they do not make a strong case for functional binocular regions in the dLGN, would not be confounded by low staining intensities.

We also looked at the retina from one fluorescently-injected subject, and found staining in all RGC cells (data not shown). There did not appear to be regions of the retina that received stronger staining than others, and other CTB-injected retinal studies do not note systematic differences in the filling of RGC cells (Matteau et al., 2003; Rainer et al., 1996; Angelucci et al., 1996).

2.5.2 Conclusion

This study supports the hypothesis that there is perhaps more detailed anatomical organization in the rat dLGN than previously described. We found evidence for three to four spatially separated ipsilateral putative subregions in the largely-contralateral dLGN, along with evidence to suggest that these regions are likely to be sampled separately from the contralateral input by dLGN relay cells. However, we did not find any cytoarchitectural differences within these layers or between subregions to suggest organization of different morphological cell types. Early work (Montero et al., 1968; Hickey and Spear, 1976; Martin, 1986; Reese, 1988) has shown that the rat dLGN can be broken down into an 'outer shell' receiving a projection of the complete contralateral visual field, and an 'inner core', which receives a projected map of the contralateral nasal retina and an island of input from the ipsilateral temporal retina. These regions have been called 'hidden laminae' due to the fact that they show no overt cytoarchitectural or myoarchitectural differences (Reese, 1988; Gabbot and Bacon, 1994). In this study, we too find that there appear to be no cell-body size, shape, orientation, staining or organizational differences within the dLGN, but these are certainly not the only characteristics one could study. By isolating and tracing of selected rat RGC subclasses instead of all RGCs simultaneously (as we have done here), one might find these hidden layers become more obvious. This is just beginning to be done in rodents, and the first studies using these techniques indeed pull out subregions in the rodent dLGN (Huberman et al., 2008, 2009; Ecker et al., 2011).

Some or all of the material presented in this chapter and in chapter 2 may be prepared for submission for publication. Discenza CB, Reinagel P. The dissertation author was the primary investigator and author of this material.

2.6 References

Abramoff, M.D., Magalhaes, P.J., & Ram, S.J. (2004). Image Processing with ImageJ. Biophotonics International, 11(7): 36-42.

Anderson, J. C., da Costa, N. M., & Martin, K. A. C. (2009). The W cell pathway to cat primary visual cortex. The Journal of Comparative Neurology, 516(1): 20-35.

Angelucci, A., Clascá, F., & Sur, M. (1996). Anterograde axonal tracing with the subunit B of cholera toxin: A highly sensitive immunohistochemical protocol for revealing fine axonal morphology in adult and neonatal brains. Journal of Neuroscience Methods, 65(1): 101-112.

Brauer, K., Winkelmann, E., Nawka, S., & Strnad, W. (1982). Comparative volumetric investigations on the lateral geniculate body of mammals. Z. Mikrosk Anat Forsch, 96: 400-406.

Carpenter, A. E., Jones, T. R., Lamprecht, M. R., Clarke, C., Kang, I. H., Friman, O., et al. (2006). CellProfiler: Image analysis software for identifying and quantifying cell phenotypes. Genome Biology, 7(10): R100.

Carvell, G. E., & Simons, D. J. (1990). Biometric analyses of vibrissal tactile discrimination in the rat. The Journal of Neuroscience : The Official Journal of the Society for Neuroscience, 10(8): 2638-2648.

Ecker, J. L., Dumitrescu, O. N., Wong, K. Y., Alam, N. M., Chen, S. K., LeGates, T., et al. (2010). Melanopsin-expressing retinal ganglion-cell photoreceptors: Cellular diversity and role in pattern vision. Neuron, 67(1): 49-60.

Fukuda, Y. (1977). A three-group classification of rat retinal ganglion cells: Histological and physiological studies. Brain Research, 119(2): 327-344.

Fuller, J. H. (1985). Eye and head movements in the pigmented rat. Vision Research, 25(8): 1121-1128.

Gabbott, P. L., & Bacon, S. J. (1994). Two types of interneuron in the dorsal lateral geniculate nucleus of the rat: A combined NADPH diaphorase histochemical and GABA immunocytochemical study. The Journal of Comparative Neurology, 350(2): 281-301.

Gabbott, P. L. A., Somogyi, J., Stewart, M. G., & Hámori, J. (1986). A quantitative investigation of the neuronal composition of the rat dorsal lateral geniculate nucleus using GABA-immunocytochemistry. Neuroscience, 19(1): 101-111.

Grieve, K. L. (2005). Binocular visual responses in cells of the rat dLGN. The Journal of Physiology, 566(1): 119-124.

Guido, W., Lu, S-M. & Sherman, S.M. (1992). Relative contributions of tonic and burst response modes to the receptive field properties of lateral geniculate neurons in the cat. Journal of Neurophysiology, 6: 2199-2211.

Guido, 2006

Hess, B. J., Precht, W., Reber, A., & Cazin, L. (1985). Horizontal optokinetic ocular nystagmus in the pigmented rat. Neuroscience, 15(1): 97-107.

Hickey, T. L., & Spear, P. D. (1976). Retinogeniculate projections in hooded and albino rats: An autoradiographic study. Experimental Brain Research. Experimentelle Hirnforschung. Experimentation Cerebrale, 24(5): 523-529.

Hikosaka, O., & Sakamoto, M. (1987). Dynamic characteristics of saccadic eye movements in the albino rat. Neuroscience Research, 4(4): 304-308.

Hill, A. J., & Best, P. J. (1981). Effects of deafness and blindness on the spatial correlates of hippocampal unit activity in the rat. Experimental Neurology, 74(1): 204-217.

Holscher, C., Schnee, A., Dahmen, H., Setia, L., & Mallot, H. A. (2005). Rats are able to navigate in virtual environments. The Journal of Experimental Biology, 208(3): 561-569.

Hubel, D. H., & Wiesel, T. N. (1961). Integrative action in the cat's lateral geniculate body. The Journal of Physiology, 155: 385-398.

Huberman, A. D., Manu, M., Koch, S. M., Susman, M. W., Lutz, A. B., Ullian, E. M., et al. (2008). Architecture and activity-mediated refinement of axonal projections from a mosaic of genetically identified retinal ganglion cells. Neuron, 59(3): 425-438.

Huberman, A. D., Wei, W., Elstrott, J., Stafford, B. K., Feller, M. B., & Barres, B. A. (2009). Genetic identification of an on-off direction- selective retinal ganglion cell subtype Reveals a layer-specific subcortical map of posterior motion. Neuron, 62(3): 327-334.

Hutson, K. A., & Masterton, R. B. (1986). The sensory contribution of a single vibrissa's cortical barrel. Journal of Neurophysiology, 56(4): 1196-1223.

Huxlin, K. R., & Goodchild, A. K. (1997). Retinal ganglion cells in the albino rat: Revised morphological classification. The Journal of Comparative Neurology, 385(2): 309-323.

Jacobs, G. H., Fenwick, J. A., & Williams, G. A. (2001). Cone-based vision of rats for ultraviolet and visible lights. The Journal of Experimental Biology, 204(14): 2439-2446.

Jeffrey, G., Cowey, A., & Kuypers, H. G. (1981). Bifurcating retinal ganglion cell axons in the rat, demonstrated by retrograde double labelling. Experimental Brain Research.Experimentelle Hirnforschung.Experimentation Cerebrale, 44(1): 34-40.

Jones, E. G. (2007). The Thalamus. New York, NY: Cambridge University Press.

Kondo, Y., Takada, M., Honda, Y., & Mizuno, N. (1993). Bilateral projections of single retinal ganglion cells to the lateral geniculate nuclei and superior colliculi in the albino rat. Brain Research, 608(2): 204-215.

Kulvicius, T., Tamosiunaite, M., Ainge, J., Dudchenko, P., & Worgotter, F. (2008). Odor supported place cell model and goal navigation in rodents. Journal of Computational Neuroscience, 25(3): 481-500.

Levick, W.R., Cleland, B. G. & Dublin, M. W. (1972) Lateral geniculate neurons of cat: retinal inputs and physiology. Invest. Ophthalmol.11(5): 302-311.

Lu, S. M., Guroo, W. & Sherman, S. M. (1992). Effects of membrane voltage on receptive field properties of lateral geniculate neurons in the cat: Contributions of the low threshold Ca2+ conductance. Journal of Neurophysiology, 6: 2185-2198.

Maaswinkel, H., & Whishaw, I. Q. (1999). Homing with locale, taxon, and dead reckoning strategies by foraging rats: Sensory hierarchy in spatial navigation. Behavioural Brain Research, 99(2): 143-152.

Marc, R. E., & Jones, B. W. (2002). Molecular phenotyping of retinal ganglion cells. The Journal of Neuroscience : The Official Journal of the Society for Neuroscience, 22(2): 413-427.

Markus, E. J., Barnes, C. A., McNaughton, B. L., Gladden, V. L., & Skaggs, W. E. (1994). Spatial information content and reliability of hippocampal CA1 neurons: Effects of visual input. Hippocampus, 4(4): 410-421.

Martin, P. R. (1986). The projection of different retinal ganglion cell classes to the dorsal lateral geniculate nucleus in the hooded rat. Experimental Brain Research, 62(1): 77-88.

Matteau, I., Boire, D., & Ptito, M. (2003). Retinal projections in the cat: A cholera toxin B subunit study. Visual Neuroscience, 20(5): 481-493.

Meier, P., & Reinagel, P. (2011). Rat performance on visual detection task modeled with divisive normalization and adaptive decision thresholds. Journal of Vision. 11(9):1-17.

Montero, V. M., Brugge, J. F., & Beitel, R. E. (1968). Relation of the visual field to the lateral geniculate body of the albino rat. Journal of Neurophysiology, 31(2), 221-236. Morris, R. (1984). Developments of a water-maze procedure for studying spatial learning in the rat. Journal of Neuroscience Methods, 11(1): 47-60.

Murray, K.D., Rubin, C.M., Jones, E.J., Chalupa, L.M. (2008). Molecular correlates of laminar differences in the Macaque dorsal lateral geniculate nucleus. Journal of Neuroscience, 28(46): 12010-12022.

Najdzion, J., Wasilewska, B., Bogus-Nowakowska, K., Równiak, M., Szteyn, S., & Robak, A. (2009). A morphometric comparative study o fthe lateral geniculate body in selected placental mammals: the common shrew, the bank vole, the rabbit, and the fox. Via Medica, 68(2): 70-78.

Pape, H.C. & Eysel, U. T. (1986). Binocular interactions in the lateral geniculate nucleus of the cat: GABAergic inhibition reduced by dominant afferent activity. Expl Brain Res. 61: 265-271.

Prusky, G. T., Harker, K. T., Douglas, R. M., & Whishaw, I. Q. (2002). Variation in visual acuity within pigmented, and between pigmented and albino rat strains. Behavioural Brain Research, 136(2): 339-348.

Reese, B. E. (1984). The projection from the optic tectum to the dorsal lateral geniculate nucleus in the rat. Brain Research, 305(1): 162-168.

Reese, B. E. (1988). 'Hidden lamination' in the dorsal lateral geniculate nucleus: The functional organization of this thalamic region in the rat. Brain Research Reviews, 13(2): 119-137.

Reese, B. E., & Cowey, A. (1983). Projection lines and the ipsilateral retinogeniculate pathway in the hooded rat. Neuroscience, 10(4): 1233-1247.

Reese, B. E., & Jeffery, G. (1983). Crossed and uncrossed visual topography in dorsal lateral geniculate nucleus of the pigmented rat. Journal of Neurophysiology, 49(4): 877-885.

Sackett, G.P., Graham, J., & DeVito, J.L. (1989). Volumetric growth of the major brain divisions in fetal macaca nemestrina. Journal für Hirnforschung, 30(4): 479-487.

Save, E., Nerad, L., & Poucet, B. (2000). Contribution of multiple sensory information to place field stability in hippocampal place cells. Hippocampus, 10(1): 64-76.

Sherman, S. M., & Guillery, R. W. (1996). Functional organization of thalamocortical relays. Journal of Neurophysiology, 76(3): 1367-1395.

Shi, C., & Davis, M. (2001). Visual pathways involved in fear conditioning measured with fear-potentiated startle: Behavioral and anatomic studies. The Journal of Neuroscience : The Official Journal of the Society for Neuroscience, 21(24): 9844-9855.

Thompson, W. R., & Solomon L. M. (1954). Spontaneous pattern discrimination in the rat. Journal of Comparative and Physiological Psychology, 47(2): 104-107.

Torborg, C. L., & Feller, M. B. (2004). Unbiased analysis of bulk axonal segregation patterns. Journal of Neuroscience Methods, 135(1-2): 17-26.

Tsumoto, T. (1990). Excitatory amino acid transmitters and their receptors in neural circuits of the cerebral neocortex. Neruosi Res, 9(2): 79-102.

Wallace, D. G., Hines, D. J., Pellis, S. M., & Whishaw, I. Q. (2002). Vestibular information is required for dead reckoning in the rat. The Journal of Neuroscience : The Official Journal of the Society for Neuroscience, 22(22): 10009-10017.

Yonehara, K., Ishikane, H., Sakuta, H., Shintani, T., Nakamura-Yonehara, K., Kamiji, N. L., et al. (2009). Identification of retinal ganglion cells and their projections involved in central transmission of information about upward and downward image motion. PloS One, 4(1): e4320.

Zoccolan, D., Oertelt, N., DiCarlo, J. J., & Cox, D. D. (2009). A rodent model for the study of invariant visual object recognition. Proceedings of the National Academy of Sciences of the United States of America, 106(21): 8748-8753.

Zoladek, L. &W.A. Roberts. (1978). The sensory basis of spatial memory in the rat. Anim. Learn. Behav. 6: 77-81.

Appendix A

Positive control of cytoarchitectural methods using macaque dLGN

A.1 CellProfiler isolates cytoarchitectural differences between functional dLGN subregions in the macaque monkey.

As a positive control for our CellProfiler cytoarchitectural methods (Carpenter et al., 2006), we passed an image of the macaque dLGN taken from Brainmaps.org (Mikula et al., 2011) through the same code that we used to analyze our rat dLGN images (Figure A.1). It is not only known that the macaque dLGN breaks down into functionally organized layers, but also that these layers display different cell-body properties when nissl or horseradish-peroxidase stained (Clark, 1932, 1941; Kaas et al., 1972, 1978). Magnocellular layers contain large cells that stain deeply, parvocellular layers contain smaller, weaker-stained cells that lie farther apart from each other, and the interleaving koniocellular layers contain cells that are even smaller and less dense (Perry et al., 1984; Shapley and Perry, 1986; see Jones, 2007 for review). As we were unable to detect any differences between subregions of the rat dLGN with regard to any of the cell-soma parameters exam-

Figure A.1: Macaque image sectioned for validating CellProfiler cytoarchitectural methods.

Magnocellular layers are outlined here with dashed lines, parvocellular layers are outlined with solid lines, and koniocellular layers lie between parvo- and magnocellular layers. These layer subregions were analyzed using the same methods as were used for the rat (see Chapter 2, Methods).

ined, we used this macaque image with its known laminar differences to validate our methods.

Indeed, when we ran the CellProfiler code with segments taken from each layer of the macaque dLGN, we found we were able to pull out clusters of image segments corresponding to the different types of macaque dLGN cells. When plotting cell size versus distance to nearest neighbor (a measure of density), we noticed that magno-, parvo-, and koniocellular regions clustered into distinct locations in the area-density space, with parvocellular cells being the smallest and least dense and magnocellular cells being the largest and most dense, as expected (see Figure A.2).

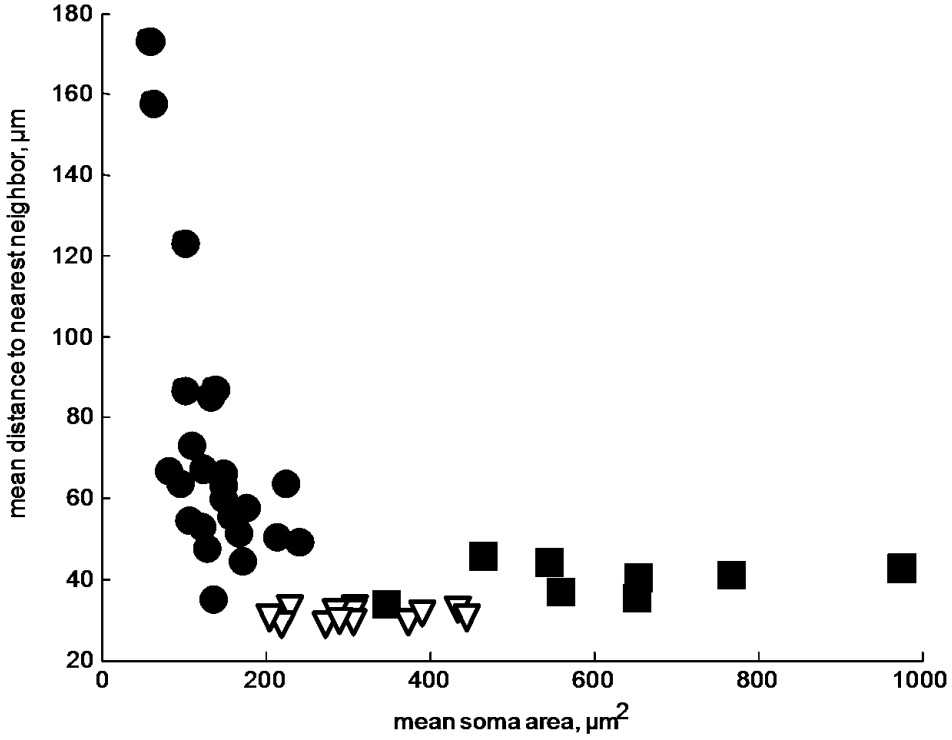

Figure A.2: Plot of mean distance to nearest neighbor versus mean cell soma area for all segments of the layers of the macaque dLGN.

Here, each shape represents the mean of the CellProfiler statistics for one portion of the segmented dLGN macaque image. Black circles represent means from koniocellular segments, white triangles represent means from parvocellular segments, and black circles represent means from magnocellular segments.

From this positive control experiment, we are able to strengthen our claim that the absence of observable cytoarchitectural distinctions between the layers of the rat dLGN come not from the inability of our anatomical methods to extract such differences, but instead arise from the apparent homogeneity of the nucleus as a whole.

A.2 References

Carpenter, A. E., Jones, T. R., Lamprecht, M. R., Clarke, C., Kang, I. H., & Friman, O. (2006). CellProfiler: Image analysis software for identifying and quantifying cell phenotypes. Genome Biology, 7(10): R100.

Clark, W.E. (1932). A morphological study of the lateral geniculate body. Brit. J. Ophthal. 16: 264-284.

Clark, W. E., & Gros, L.E. (1941). The laminar organization and cell content of the lateral geniculate body in the monkey. J.Anat., Lond. 75: 419-433.

Jones, E. G. (2007). The Thalamus. New York, NY: Cambridge University Press.

Kaas, J.H., Guillery, R.W. & Allman, J.M. (1972). Some principles of organization in the dorsal lateral geniculate nucleus. Brain, Behav. Evol. 6: 253-299.

Kaas, J.H., Huerta, M.F., Weber, J.T., & Harting, J.K. (1978). Patterns of retinal terminations and laminar organization of the lateral geniculate nucleus of primates. J. Comp. Neurol. 182: 517-553.

Miklula, S., Stone, J.M., Berman, A.L., & Jones, E.G. (2011). A digital sterotaxic atlas of the brain of the monkey, Macaca mulatta. Brainmaps.org. Supported by the Human Brain Project of the National Institutes of Health, United States Public Health Service.

Perry, V.H., Oehler, R., & Cowey, A. (1984). Retinal ganglion cells that project to the dorsal lateral geniculate nucleus in the macaque monkey. Neuroscience. 12(4): 1101-1123.

Shapley, R.M., & Perry, V.H. (1986). Cat and monkey retinal ganglion cells and their visual functional roles. Trends Neurosci. 9: 1-7.